January 2013

Intraocular Pressure, Aqueous Humor Dynamics, And Fibrosis Using A Novel Glaucoma Drainage Pathway

Julius Oatts

INTRAOCULAR PRESSURE, AQUEOUS HUMOR DYNAMICS, AND FIBROSIS USING A NOVEL GLAUCOMA DRAINAGE PATHWAY

A Thesis Submitted to the
Yale University School of Medicine
in Partial Fulfillment of the Requirements for the
Degree of Doctor of Medicine

by
Julius Thomas Oatts
Class of 2013

INTRAOCULAR PRESSURE, AQUEOUS HUMOR DYNAMICS, AND FIBROSIS USING A NOVEL GLAUCOMA DRAINAGE PATHWAY.

Julius T. Oatts, Ze Zhang, Harry Tseng, M. Bruce Shields, John H. Sinard, Nils A. Loewen. Department of Ophthalmology and Visual Sciences, Yale University, School of Medicine, New Haven, CT.

The purpose of this study was to compare fibrosis, aqueous humor dynamics, and intraocular pressure (IOP) of two suprachoroidal shunts that are part of a new class of glaucoma drainage devices. After in vitro testing, 20 rabbits were implanted with either a gold shunt (GS, GMSplus+, Solx) or polypropylene shunt (PS, Aquashunt, OPKO). Ten eyes received mitomycin C (MMC) and triamcinolone. Peak and trough IOP were monitored with a pneumatonometer and tono-pen through 15 weeks. Aqueous humor dynamics were evaluated fluorophotometrically and tonographically. Fibrosis was quantified using ImageJ. In vitro growth was similar. In vivo, both shunts were devoid of foreign body reaction but exhibited fibrosis, and GS showed vascularization. There was no significant difference in aqueous or uveoscleral flow. Preoperative morning IOP was 23.7 ± 2 mm Hg and evening IOP was 26.5 ± 2 mm Hg (p=0.000). Morning IOP was decreased through 15 weeks and evening IOP through 8 weeks in all groups. The morning IOP decrease was most profound at 15 weeks in PS (41%) compared to GS (18%). Antifibrotics initially enhanced but eventually diminished shunt performance. At 15 weeks, thickness of scleral fibrosis was greater in GS (246 ± 47 μ) and PS (188 ± 47 μ, p=0.285) compared with GS+MMC (109 ± 26 μ, p=0.023 to GS) and PS+MMC (48 ± 30 μ, p=0.028 to PS). In a rabbit model, suprachoroidal polypropylene and gold shunts allow access to a new drainage pathway with different IOP profiles that can be modified with antifibrotics.

ACKNOWLEDGEMENTS

I am deeply indebted to Dr. Nils Loewen for unmatched mentorship which often extended beyond our work in the laboratory together. He embodies a critical thinker and used this skill to improve both our project and me as a scientist. He went above and beyond what was expected of him and served as an invaluable and always available resource, whether in a lab meeting, or on a Friday night. As I finished my year of research, Dr. Loewen also made a transition - to leave Yale. While he will be a sorely missed presence in the ophthalmology department here, I am certain he has many years of scientific accomplishment and meaningful mentoring ahead of him, and I look forward to regarding him as one of my personal mentors and role models for the entirety of my career as an ophthalmologist.

Ze Zhang and Harry Tseng are responsible for the in vitro biocompatibility portion of this project, and I am thankful for their resourceful work which added an interesting perspective to this project.

I would like to thank Dr. Sinard for his eager willingness to join our project and his expertise on the intricacies of the eye. He provided crucial ideas and insights into our project design and was extremely receptive to collaboration and served as an integral part of this project.

This project would not have been possible without my thesis committee, Dr. Ron Adelman, Dr. Tomas Grippo, and Dr. Jimmy Zhou. Thanks are also due to Donna Carranzo and Mae Geter, who tirelessly work with students to ensure their research has a healthy environment in which to flourish. I would also like to thank Dr. Forrest for his dedication to scientific research. Katie McFarland was an integral part of the logistics supporting this work, and many steps literally would not have been completed if it weren't for her steadfast dedication to getting the job done.

We would like to acknowledge the Office of Student Research as well as the Department of Ophthalmology for funds which were used for this project. We would also like to thank Dr. Bruce Shields and SOLX, Inc for providing the glaucoma drainage devices described in this thesis. We would also like to thank Mrs. Cecilia Teitell and Mr. Ernest F. Teitell for their generous support. I would like to confirm the use of original photography for the images presented in this thesis.

Finally, I would like to thank my family and friends for their support during this exciting process.

TABLE OF CONTENTS

INTRODUCTION

Glaucoma is the leading cause of irreversible blindness in those of African and Latino descent, and the second leading cause among Caucasians.[1] The increasing burden of glaucoma is a direct result of higher life expectancy[2] and the considerable risks of standard trabeculectomy and glaucoma drainage device procedures.[3] This has led to a search for new surgical treatment modalities for moderate and advanced disease stages aimed at preventing the disease's long-term sequelae. Trabeculectomy remains the most commonly used penetrating procedure for glaucoma, and the surgical standard of care for moderate to advanced glaucoma.[4] Because classical glaucoma surgeries shunt aqueous humor to a subconjunctival or sub-Tenon pocket ("bleb") on the outside of the eye, fibrosis and infection remain a lifelong threat.[3] It follows that these procedures have many associated complications including bleb leaks, bleb infections, and bleb fibrosis. A high failure and complication rate has led to the use of adjuvant antifibrotic agents in addition to novel drainage devices such as tube-shunts.[5] Even with the addition of Mitomycin C (MMC), a potent antifibrotic agent, the complication rate remains high, most notably increasing the life-long risk of vision-threatening endophthalmitis.[6]

A recently introduced novel approach to glaucoma surgery involves creating a communication between the anterior chamber and the suprachoroidal space through the use of a suprachoroidal shunt. Suprachoroidal shunts have been developed in an attempt to avoid the complications of conventional drainage devices by draining aqueous humor into a potential space on the inside of the eye, the suprachoroidal space, taking advantage of the natural hydrostatic pressure gradient between the anterior chamber and the suprachoroidal space.[7] Drainage into the suprachoroidal space has the theoretical potential to profoundly lower intraocular pressure (IOP) through increasing uveoscleral

pathway outflow; however, given the newness of this technology, long-term outcomes data is not available in humans or animals.[8]

Risk of glaucomatous visual field progression correlates with IOP variability,[9,10] therefore an evaluation of IOP variability is useful in assessing novel glaucoma treatments. More specifically, characteristic changes have been reported in 24-hour IOP monitoring of early glaucomatous eyes: higher diurnal IOP's as well as smaller differences in diurnal-to-nocturnal IOP change.[11] Diurnal IOP variation has been widely reported in the literature, with peaks occurring in the morning, even in normal subjects.[12,13] Prostaglandins have been shown to lower both nocturnal and diurnal IOP,[14] presumably by increasing outflow through the uveoscleral pathway.[15] This suggests that nocturnal pressures may be particularly useful to study uveoscleral outflow.

In this study, we compared two suprachoroidal shunts, a gold shunt (GS; GMSplus+; SOLX Ltd., Waltham, MA) and a polypropylene shunt (PS; Aquashunt; OPKO Health, Miami, FL), examining in vitro and in vivo growth patterns of the cell types that come into direct contact with these devices. Using rabbits as a species that has very little natural uveoscleral outflow, we hypothesized that we could create a fibrosis-prone animal model to readily display differences in shunt function and the impact of antifibrotics on outflow.

Because suprachoroidal shunts increase flow into the anatomic compartment that is primarily responsible for pressure-independent, uveoscleral outflow, we hypothesized that suprachoroidal shunts would reduce IOP the most at a time of the day when this outflow contributes the least.

HYPOTHESIS

Suprachoroidal shunts provide a theoretically feasible approach to lowering eye pressure in the treatment of glaucoma, and we hypothesized these devices will lower eye pressure through increasing aqueous outflow in normotensive rabbits. Because the success of glaucoma surgery depends on postoperative wound healing and amount of scar tissue formation, we proposed that differences in eye pressure lowering between the gold shunt (GS) and polypropylene shunt (PS) would be a factor of differential fibrosis. In animals receiving anti-fibrotics (mitomycin C, MMC and triamcinolone, TAC) at the time of shunt implantation, we expected to see more profound pressure lowering and a smaller degree of fibrosis.

SPECIFIC AIMS

1. Establishment of a Suprachoroidal Shunt Fibrosis Model in the Rabbit

To establish a suprachoroidal shunt model in the rabbit that allows the comparison of different shunt designs and materials (GS and PS) and the usefulness of two modulators of fibrosis and wound healing (MMC and TAC).

2. Shunt Effect on Aqueous Humor Dynamics and Intraocular Pressure

To assess the effect of GS and PS implantation on fluorophotometric and tonographic outflow facility, uveoscleral flow and intraocular pressure in rabbits with and without MMC and TAC.

METHODS

In Vitro Proliferation Studies

In vitro biocompatibility of suprachoroidal shunts was evaluated using cell lines of corneal endothelial, trabecular meshwork, and fibroblast origin that were transduced with feline immunodeficiency viral (FIV) vectors to stably express enhanced green fluorescent protein (eGFP) as described previously.[16-21] Briefly, feline kidney fibroblast (CrFK) (ATCC, Manassas, VA), trabecular meshwork (NTM5) (gift from Alcon, Fort Worth, TX), and bovine corneal endothelial (BCE) (ATCC, Manassas, VA) cells were transduced with a multiplicity of infection (MOI) of 30 to achieve high and even expression levels followed by expansion.[16]

eGFP-expressing CrFK, BCE, and NTM5 cells were seeded onto GS and PS inside 6-well plates at 75 cells mm^2. Growth rate on these materials was compared to that of control wells by eGFP-optimized fluorescent image capture (Eclipse TE300; Nikon, Melville, NY).

Study Design

Right eyes of 20 rabbits were implanted with GS or PS **(Figure 1)** to have an 89% chance of detecting IOP difference of 3 ± 2 mm Hg or 93% for 5 ± 2 mm Hg (non-paired t-test, alpha error 5%). GS was the most recent generation device (GMSplus+; SOLX Ltd., Waltham, MA) with an external size of 3.2 x 5.2 x .05 mm^3 while PS (Aquashunt; OPKO Health, Miami, FL) had an external size of 4 x 10 x .75 mm^3. Half of each group (n = 5) received intraoperative, subconjunctival mitomycin C (MMC, 0.2mg; Gemini Bio-Products, West Sacramento, CA) and intra-cyclodialysis cleft triamcinolone acetate (TAC, Triesence; Alcon Laboratories, Fort Worth, TX) to maximize antifibrotic and anti-

inflammatory action. IOP was measured with both a pneumatonometer and tono-pen preoperatively and weekly postoperatively at peak and trough times for 15 weeks. Pneumatonometry and fluorophotometry were used to measure aqueous humor turnover and calculate outflow facility and uveoscleral flow. Fibrosis was analyzed and quantified using histology and morphometry at 15 weeks postoperatively.

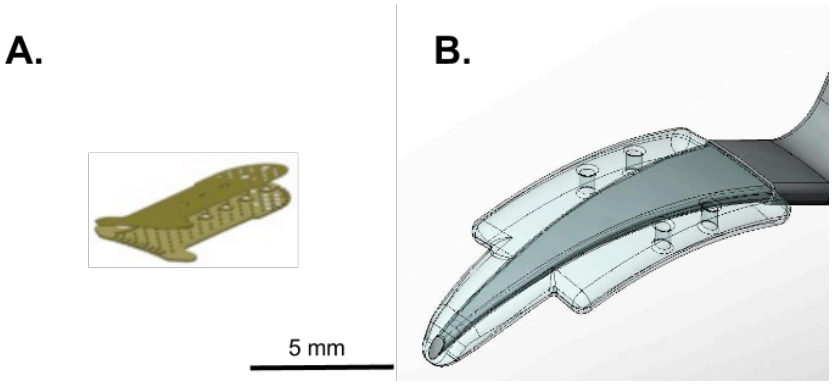

Figure 1. Suprachoroidal shunts in comparison: A, gold shunt (GS); B, polypropylene shunt (PS) on device inserter.

Animals

Shunts were implanted in 6 to 7 week-old New Zealand white rabbits (Harlan, Indianapolis, IN) that were acclimatized for 1 week to a 12-hour light-dark cycle, with lights on at 7 AM at a room temperature of 20 ± 4°C, housed in separate cages with food and water available ad libitum. All practices complied with the ARVO Statement for the Use of Animals in Ophthalmic and Vision Research and approved by the Yale University Institutional Animal Care and Use Committee.

Suprachoroidal Shunt Implantation

Animals were anesthetized with intramuscular ketamine (35 mg/kg; McKesson, San Francisco, CA) and xylazine (5 mg/kg; Lloyd, Inc., Shenandoah, IA). The surgical eye was cleaned with ophthalmic beta-iodine (Betadine 5%; Alcon Laboratories, Fort

Worth, TX), draped sterilely and a lid speculum was inserted. When macroscopic, microscopic and functional data in pilot animals confirmed that a clear corneal insertion technique from within the anterior chamber was less traumatic and more reproducible than the transscleral approach used in humans, 20 animals were implanted using this new approach. A shelved, peripheral clear corneal incision was fashioned according to shunt size. The anterior chamber at the incision site was filled by 30% with viscoelastic (Ocucoat; Bausch & Lomb, Clearwater, FL) before the tip of the cannula was turned toward the iris root and used to gently create a cyclodialysis, injecting viscoelastic to safely expand this space. Shunts were delivered to the anterior chamber via the included inserter and then carefully retracted into the cyclodialysis cleft using a cystotome **(Figure 2)**. The incision was closed with a 10-0 nylon suture. Half of each group of animals received 50 μL of TAC in the suprachoroidal space. This transscleral injection was aimed at the midsection of the shunt using a 27 gauge needle in posterior, bevel down position and applied after watertight closure when the eye was pressurized. These animals also received a subconjunctival injection of MMC. Postoperatively, all animals received moxifloxacin (Vigamox 0.5%; Alcon Laboratories, Fort Worth, TX) and prednisolone acetate 1% (Falcon Pharmaceuticals, Fort Worth, TX) every 12 hours for 7 days. Immediately postoperatively, a slit lamp exam was performed to assess for ocular inflammation (cells or flare), corneal edema, or hyphema. This exam was also repeated at 1 week.

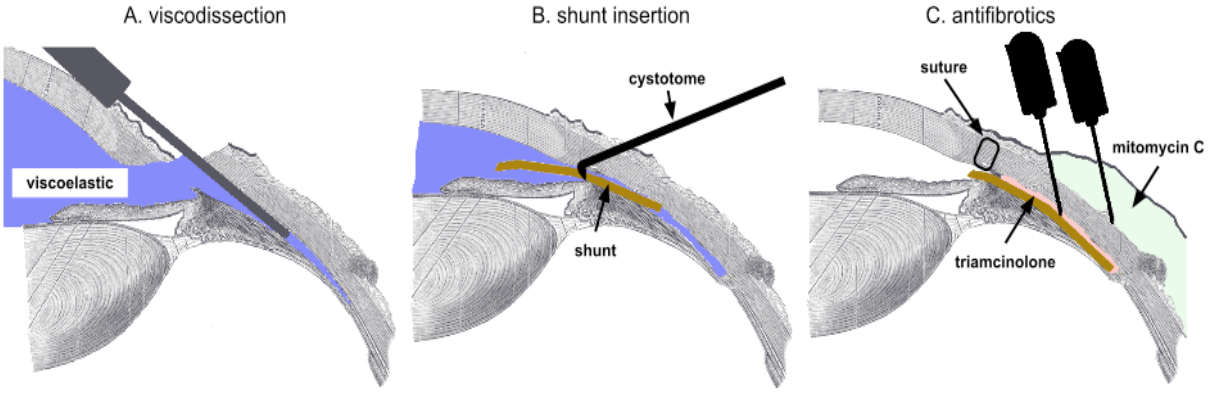

Figure 2. Suprachoroidal shunt implantation technique. (A) Following dissection of the suprachoroidal space with viscoelastic (blue), shunts were delivered into the anterior chamber and, (B) retracted with a cystotome into the pocket of viscoelastic. (C) After closing the eye, a small amount of triamcinolone (pink) and mitomycin C (green) were injected (Step 3 was included in only 10 animals).

Structural Assessment

Device placement was confirmed by ultrasound biomicroscopy (UBM) (UBM Plus; Accutome, Malvern, PA). Following anesthesia, a 20 mm eye cup was inserted between the eyelids and filled with saline solution. With a 48 MHz transducer, scanning was performed under standardized room lighting conditions. Cross-sectional and transverse images were obtained detailing the device in relation to the suprachoroidal space as well as other anatomical landmarks including cornea, iris, ciliary body, anterior chamber angle, and peripheral sclera. Central corneal thickness (CCT) was measured by ultrasound pachymetry (Pachmate; DGH Technology, Exton, PA) in triplicate in the morning and evening, corresponding with peak and trough IOP measurements.[22]

Functional Assessment

IOP measurements were performed in conscious rabbits gently restrained by hand. Rabbits received one drop of topical anesthesia with proparacaine 0.5% (Akorn,

Inc., Lake Forest, IL). All pressures were obtained using both pneumotonometry (Model 30 Pneumatonometer; Reichert Technologies, Depew, NY) and tono-pen applanation (Tono-Pen Avia; Reichert Technologies, Depew, NY) during the same measurement session.

Animals were acclimated to IOP measurements daily for 1 week before preoperative diurnal pressures were recorded. IOP was measured every 3 hours from 0800 until 2300 for 48 hours to establish preoperative diurnal patterns. IOP was then measured weekly at peak and trough pressure through 15 weeks postoperatively. Because IOP measured with the pneumatonometer was considerably higher throughout the day and more sensitively displayed circadian IOP fluctuation than measurements with the tono-pen **(Figure 3)**, statistical analysis was carried out with pneumatonometric data.

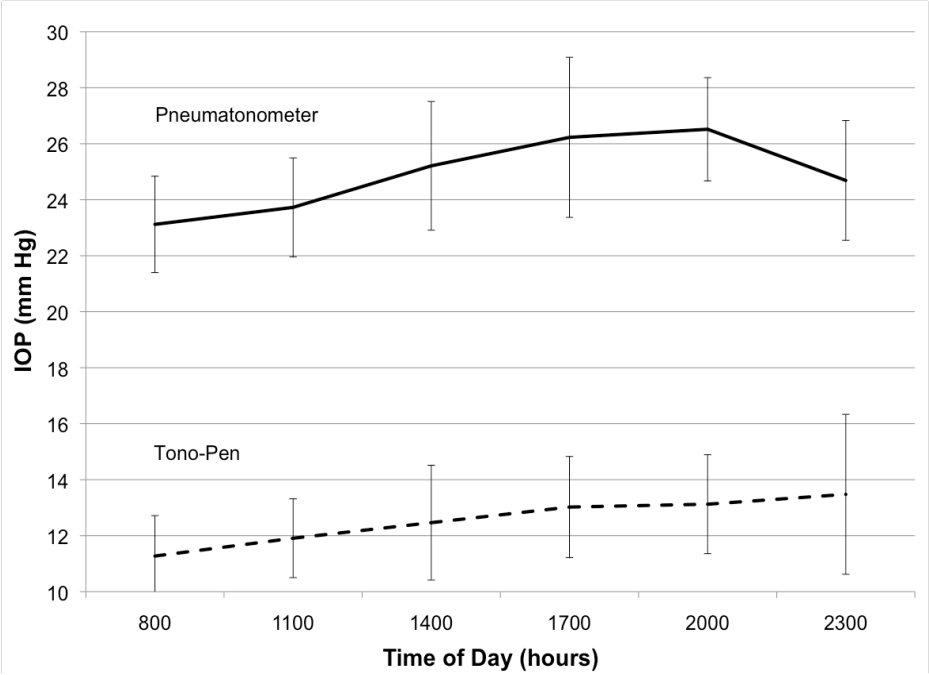

Figure 3. Preoperative IOP as measured with pneumatonometry and tono-pen in the same session.

Aqueous humor dynamics were evaluated with fluorophotometry and tonography. Aqueous turnover can be determined by staining the cornea with fluorescein eye drops

and monitoring diffusion and washout. Three hours prior to the first measurement, 5 drops of 0.25% fluorescein (Altaire Pharmaceuticals, Inc., Aquebogue, NY) were topically applied to each eye of the rabbits in 5-minute intervals. One and a half hours after the last fluorescein drop was administered, eyes were rinsed with balanced salt solution to remove excess fluorescein from the preocular tear film. Forelimb paws were also rinsed to prevent fluorescein reintroduction to the tear film through eye rubbing. The fluorescence of the cornea and anterior chamber was measured in triplicate with a scanning ocular fluorophotometer (Fluorotron Master; OcuMetrics, Mountain View, CA). Measurements were taken between 1000 and 1800. Scans were repeated at one hour intervals for four sets of scans. These data were used to determine aqueous flow (F_a).[22] Following the fourth measurement, animals received intramuscular acetazolamide (16 mg/kg; X-Gen Pharmaceuticals, Big Flats, NY) to suppress aqueous humor formation. Carbonic anhydrase inhibitors such as acetazolamide decrease IOP by reducing aqueous flow without affecting outflow variables.[23,24] Here, acetazolamide was used to calculate fluorophotometric outflow facility (C_{fl}). Two hours after this injection, animals underwent two more sets of scans, one hour apart. IOP was measured at the time of injection and subsequent scans. C_{fl} was calculated as the ratio of the change in aqueous flow to the change in IOP, $C_{flx}=(F_a-F_{ax})/(IOP-IOP_x)$, where *x* indicates the interval and F_a indicates aqueous flow.[25,26]

Tonographic outflow facility (C_{ton}) was evaluated by 2-minute constant-pressure tonography and calculated as the ratio of the change in aqueous volume to the change in IOP during the 2-minute measurement.[27] Uveoscleral outflow (F_u) was calculated using the modified Goldmann equation: $F_u = F_a - C(IOP - P_{ev})$, where C was either fluorophotometric (C_{fl}) or tonographic (C_{ton}) outflow facility (F_a = aqueous flow by

fluorophotometry; P_{ev} = episcleral venous pressure). Given the limitations of non-invasive measurement of P_{ev}, F_u was calculated using 12 mm Hg, as previously reported for rabbits.[28] When C_{fl} was used, IOP was measured prior to acetazolamide administration; when C_{ton} was used, IOP was the pneumatonometric IOP before the start of tonography.

Histology

At the study endpoint of 15 weeks, eyes of euthanized animals (120 mg/kg phenobarbital via ear vein, Euthasol; Virbac, Fort Worth, TX) were enucleated and fixed in 10% formalin for 2-3 days. After fixation, the eyes were hemisected and stereomicroscopy was performed. The device and surrounding tissue were excised as a block, processed, and paraffin embedded. Sequential 5 μm sections were cut and stained with hematoxylin and eosin (H&E). Thirty minutes prior to sacrifice, 2 to 3 anesthetized rabbits in each group received a 0.2 ml intracameral cationic ferritin tracer (10 mg/mL, pH 5.8; Sigma-Aldrich, St. Louis, MO) to assess outflow function by histology.[29] In addition to standard H&E staining, these slides were also stained with Prussian blue to highlight ferritin deposition.

Fibrosis was measured on both scleral and choroidal sides of the shunt using ImageJ 1.46 (NIH, Bethesda, MD) on digital photomicrographs. Due to the difference in cellular architecture, fibrotic tissue developing following insertion of the device was easily differentiated from normal sclera and choroid. All measurements were taken in the middle of the device, and reported values were obtained as the average of fibrosis thickness across three sections from each specimen.

Statistics

IOP, outflow facility, and uveoscleral flow were analyzed with repeated-measures analysis of variance (ANOVA). Student's paired t-tests were used to compare diurnal IOP, aqueous flow, outflow facility (both fluorophotometric and tonographic), uveoscleral flow, and central corneal thickness intraindividually. Student's unpaired t-tests were used to compare these parameters and fibrosis between groups. All data are presented as the mean ± standard deviation (SD) and were considered statistically significant at $P<0.05$.

RESULTS

1. Establishment of a Suprachoroidal Shunt Fibrosis Model in the Rabbit

In vitro biocompatibility studies presented here were primarily performed by coauthors Ze Zhang and Harry Tseng.

In Vitro Biocompatibility

All three cell types: fibroblasts (CrFK cells), trabecular meshwork cells (NTM5 cells), and corneal endothelial cells (BCE cells) seeded on both gold **(Figure 4)** and polypropylene **(Figure 5)** grew readily and reached 100% confluence within 5 days of seeding and were visualized by expression of eGFP.

Based on daily visual examination under a fluorescent microscope with an eGFP-optimized filter cube, CrFK, NTM5, and BCE cells seeded on gold and polypropylene exhibited no signs of cytotoxicity or restricted growth compared to cells seeded on the control tissue culture well. Image analysis showed that there were no significant

differences in growth rates between cells seeded on gold, polypropylene, or control tissue culture plate materials **(Figures 6, 7)**.

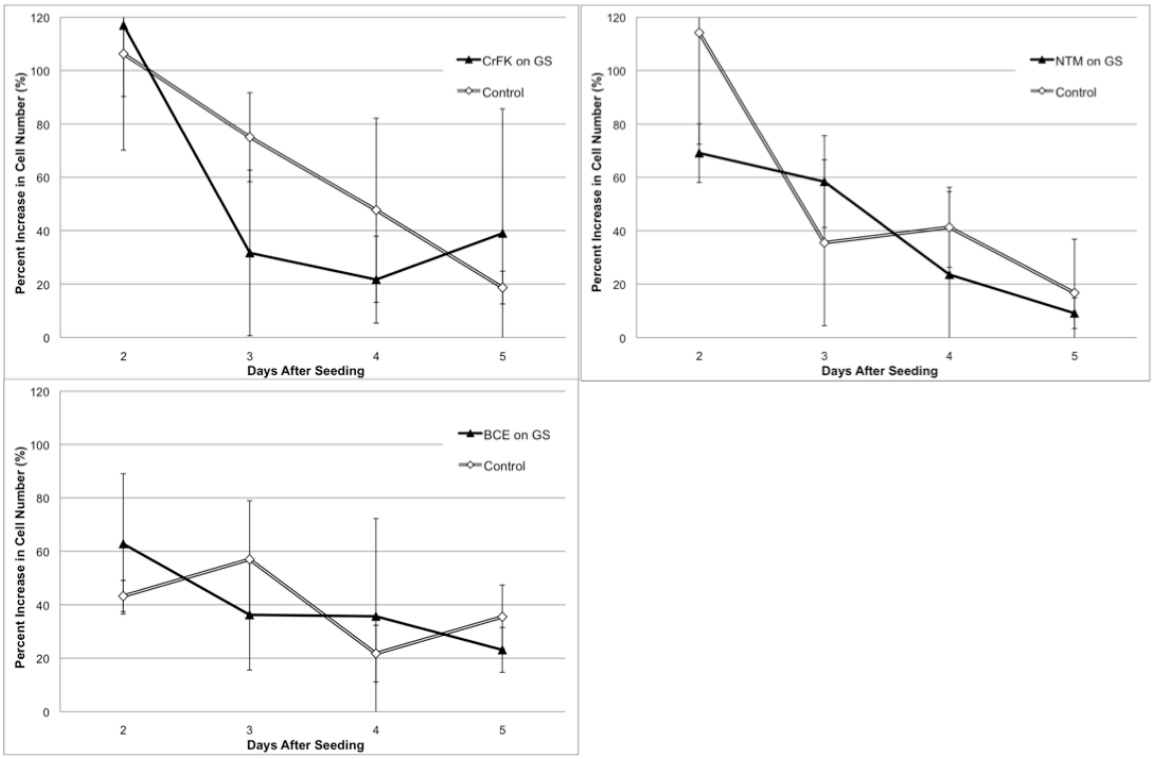

Figure 4. Cell growth rate days 2-5 after cell seeding on gold shunt (GS) compared to control (A, CrFK; B, NTM; C, BCE). (N=3)

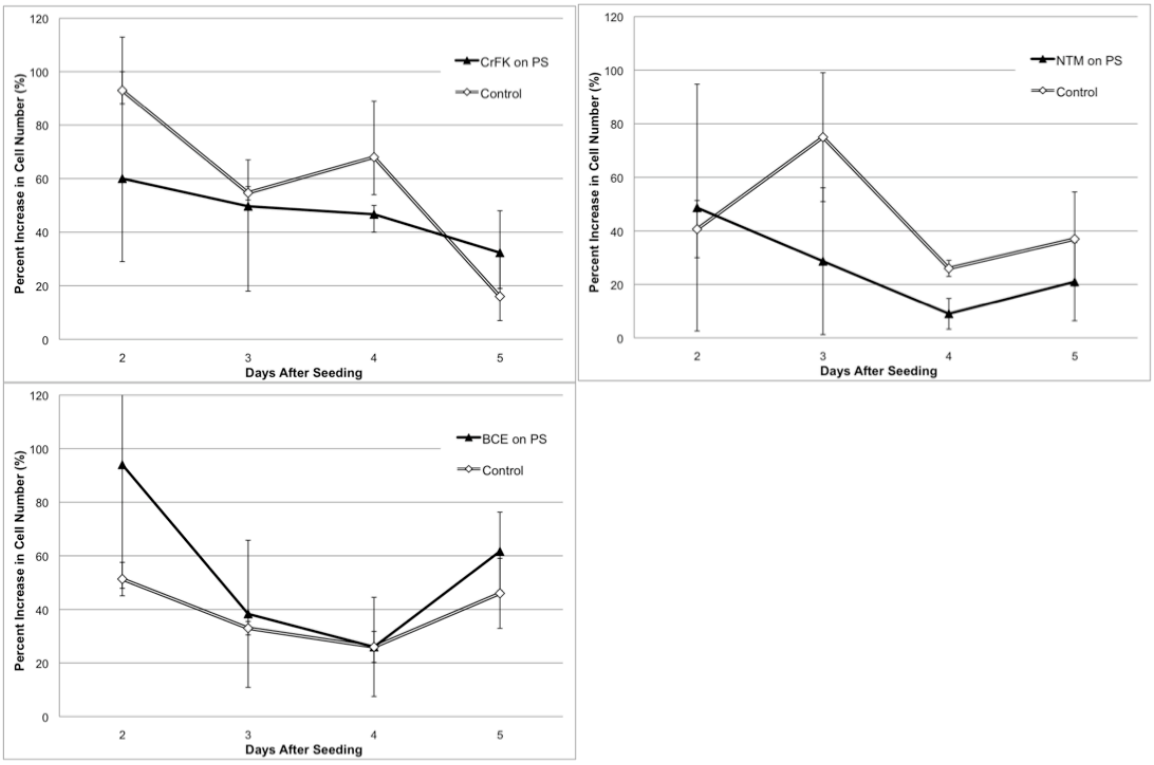

Figure 5. Cell growth rate days 2-5 after cell seeding on polypropylene shunt (PS) compared to control (A, CRFK; B, NTM; C, BCE). (N=3)

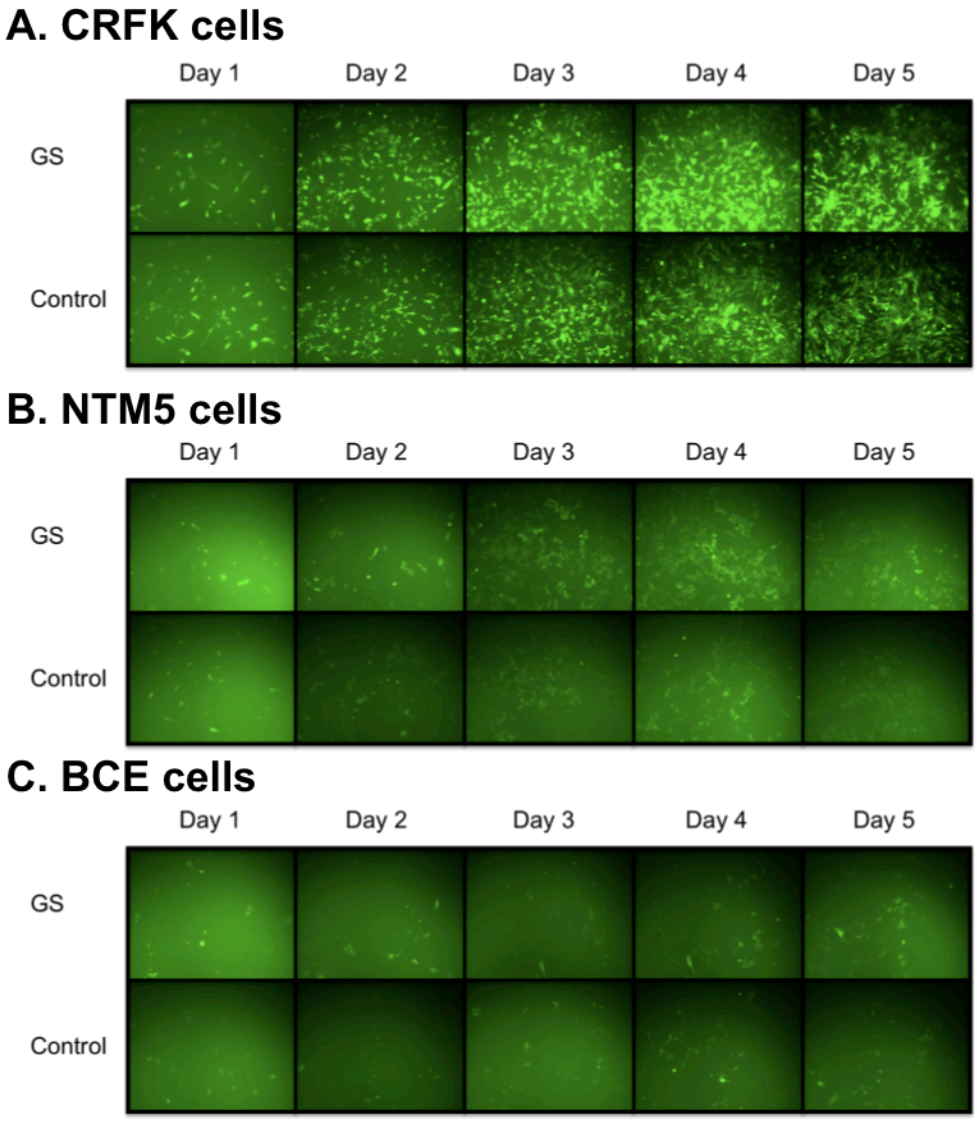

Figure 6. Progression of cell growth on gold shunt (GS) compared to control in CRFK cells (A), NTM5 cells (B), and BCE cells (C).

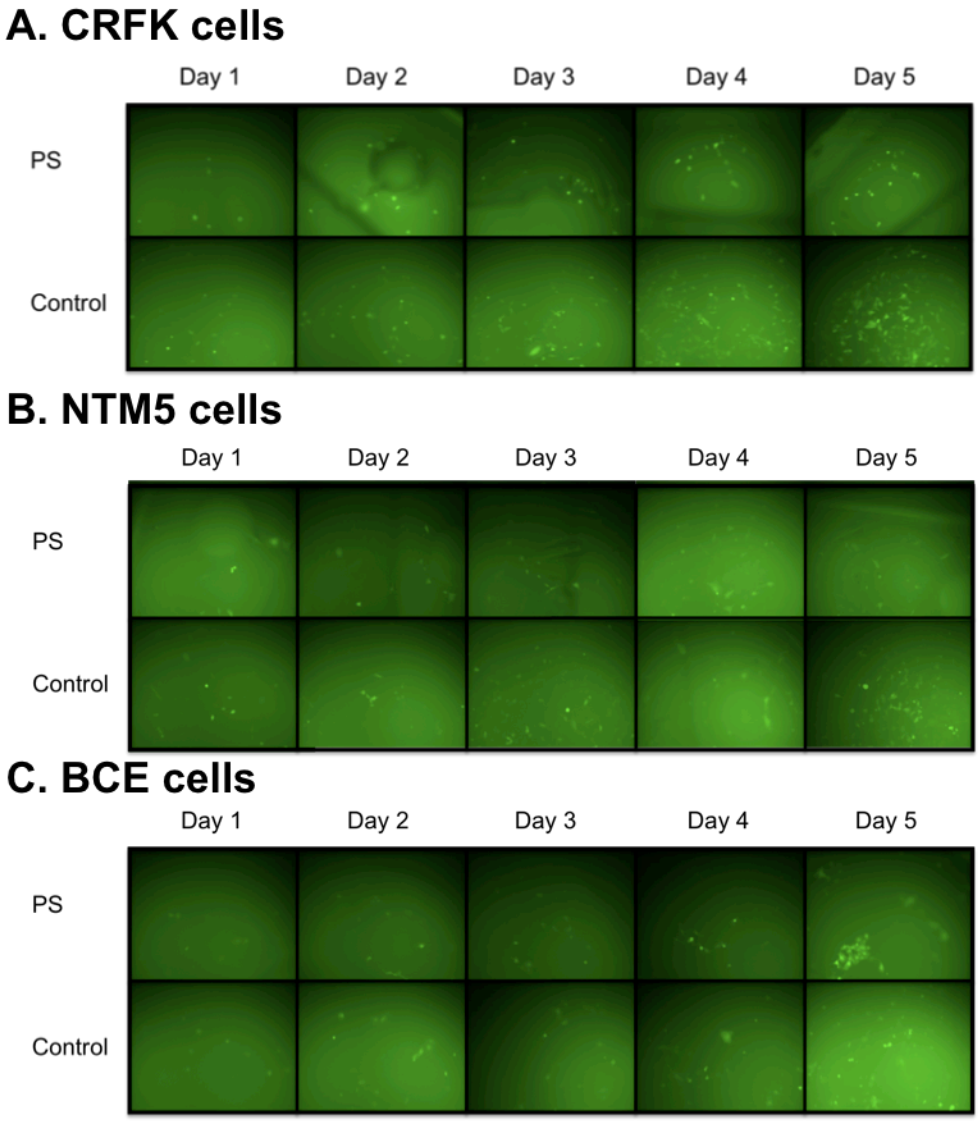

Figure 7. Progression of cell growth on polypropylene shunt (PS) compared to control in CRFK cells (A), NTM5 cells (B), and BCE cells (C).

Suprachoroidal Shunt Implantation

Two pilot animals served to develop an ab interno, intracameral, suprachoroidal shunt implantation technique for the rabbit when transscleral insertion was found to be traumatic and highly variable in this species. Implantation took approximately 20 minutes in each of the 20 subsequent animals. A limited intraoperative hyphema was observed in

5 animals, 4 of which were eyes implanted with PS. One animal experienced a retinal detachment secondary to PS implantation. Of 10 PS implanted, 2 progressively migrated towards the anterior chamber. Of the 10 animals treated with adjuvant MMC and TAC, 3 implanted with GS had shallow, diffuse blebs during the early postoperative period, two of which resolved within 2 weeks postoperatively. In the third GS animal, the bleb persisted until postoperative week 6, at which point the IOP increased **(Figure 8)**. One PS animal without MMC and TAC also had a postoperative bleb.

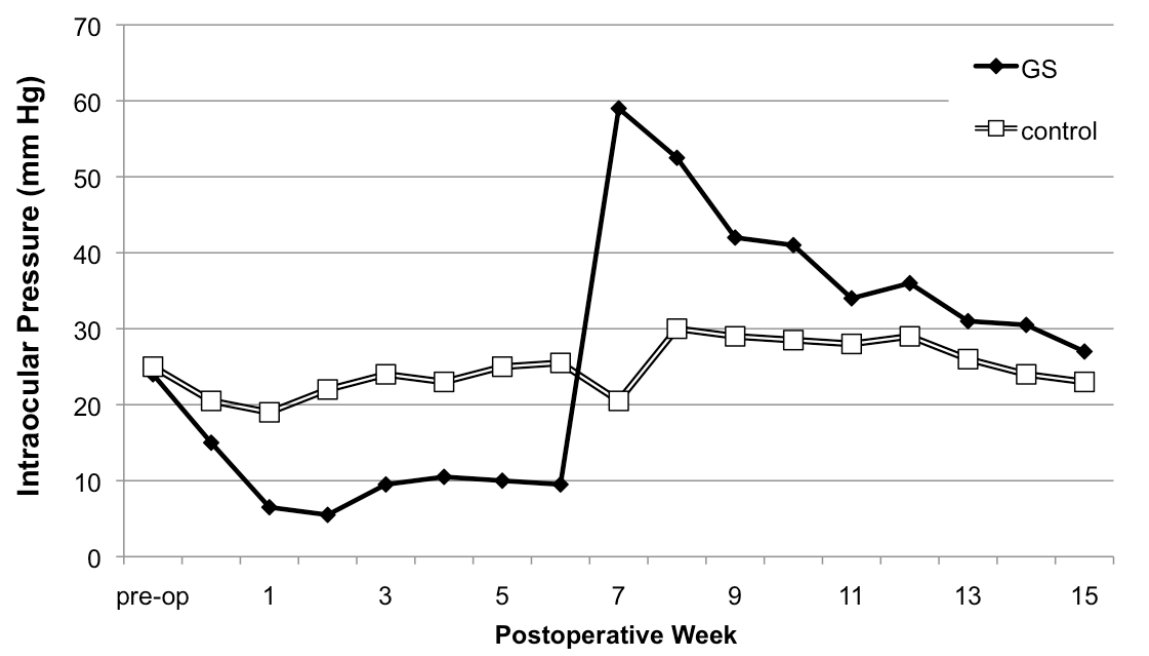

Figure 8. Postoperative intraocular pressure of a GS animal with a persistent bleb through week 6, with an unexplained pressure increase following resolution of the bleb.

Ultrasound Biomicroscopy (UBM)

UBM **(Figure 9)** with visualization of suprachoroidal lakes **(Figure 9C)** and stereomicroscopic examination **(Figure 11, 12)** confirmed implantation in the suprachoroidal space.

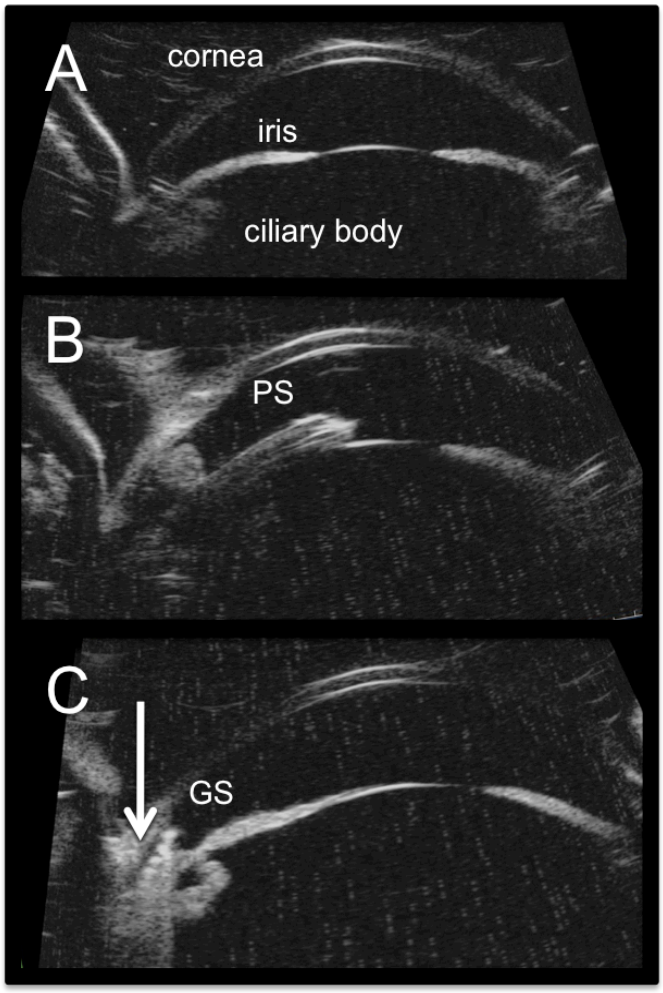

Figure 9. Ultrasound biomicroscopy showing polypropylene shunt, PS (B) and gold shunt, GS (C) in the suprachoroidal space. A suprachoroidal pocket was also visualized in GS eyes (C; arrow).

Pachymetry

No adverse effects on corneal endothelial function as measured by CCT was observed. Rabbits exhibited a diurnal variation in CCT with preoperative morning CCT of 362 ± 15 μm, and evening CCT of 333 ± 12 μm. In all groups, physiologic diurnal differences with CCT larger in the morning than in the evening were maintained through 3 months postoperatively. Device implantation had no effect on corneal thickness through 3 months **(Figure 10)**. Compared to control eyes, CCT in implanted eyes was not

significantly different at 1 month (GS, p=0.307; PS, p=0.918) or 3 months (GS, p=0.772; PS=0.663). Similarly, evening CCT was not significantly different at 1 month (GS, p=0.341; PS, p=0.982) or 3 months (GS, p=0.165; PS=0.462) **(Table 1)**.

Table 1. Central corneal thickness preoperatively and postoperatively compared between and within groups through postoperative month 3.

	GS (n=10)					**PS** (n=10)					**Control** (n=20)		
	AM	**PM**	**p**	**p***	**p****	**AM**	**PM**	**p**	**p***	**p****	**AM**	**PM**	**p**
Preoperative	368	338	0.002	0.285	0.160	360	334	0.012	0.924	0.607	359	331	0.000
Postoperative 1 month	387	365	0.143	0.307	0.341	360	340	0.005	0.918	0.982	360	347	0.029
Postoperative 3 months	368	338	0.003	0.772	0.165	360	334	0.003	0.663	0.462	378	356	0.000

p, comparing values within groups; paired, two-tailed t-test.
*p, comparing morning values to control; unpaired, two-tailed t-test
**p, comparing evening values to control; unpaired, two-tailed t-test

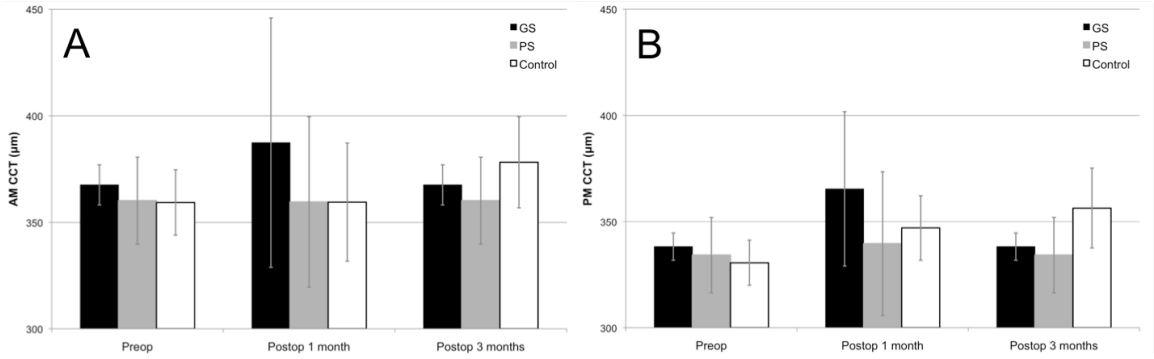

Figure 10. Morning (A) and Evening (B) central corneal thickness (CCT) showing no significant difference between groups through 3 months postoperatively.

Stereomicroscopy

Stereomicroscopy of dissected eyes confirmed proper device placement in all animals **(Figure 11)**.

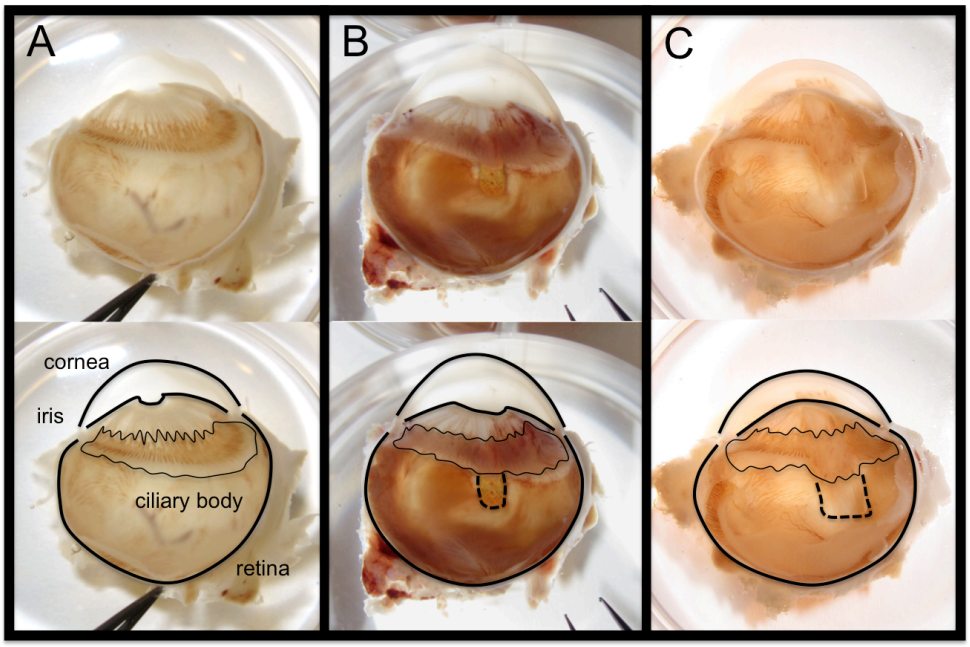

Figure 11. Stereomicroscopy confirming device placement of GS (B) and PS (C) compared to control eye (A). Duplicate images, with anatomy annotated in bottom half of panel.

Stereomicroscopy revealed a round suprachoroidal drainage pocket in one animal with a GS **(Figure 12A)**. This was not seen in any animals with PS. Other findings included vascularization that was evident at low power microscopy surrounding the posterior pole of a PS **(Figure 12B)** and a GS device **(Figure 12C)**, respectively. One retinal detachment was seen in a PS eye **(Figure 12D)**.

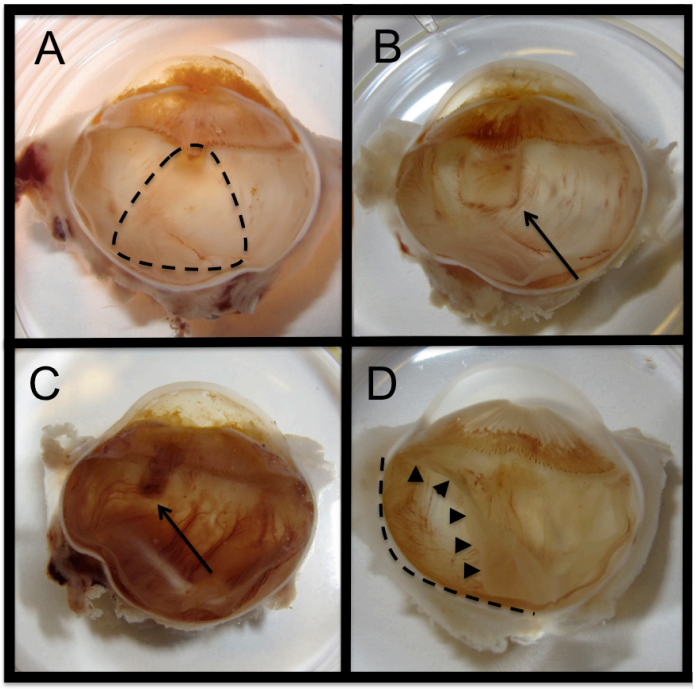

Figure 12. Side effects and complications of suprachoroidal shunt implantation. GS with suprachoroidal pocket (A; dotted circle); vascularization in PS and GS (B, C; arrow); retinal detachment in PS (D; dotted line - choroid, arrowheads - detached retina).

The GS-implanted eye of the animal with the persistent bleb through week 6 showed significant glaucomatous optic nerve cupping, a hallmark of advanced glaucoma, extensive anterior synechiae (adhesions between the peripheral iris and structures of the anterior chamber angle such as trabecular meshwork, Schwalbe's line or cornea), and corresponding buphthalmic changes **(Figure 13)**.

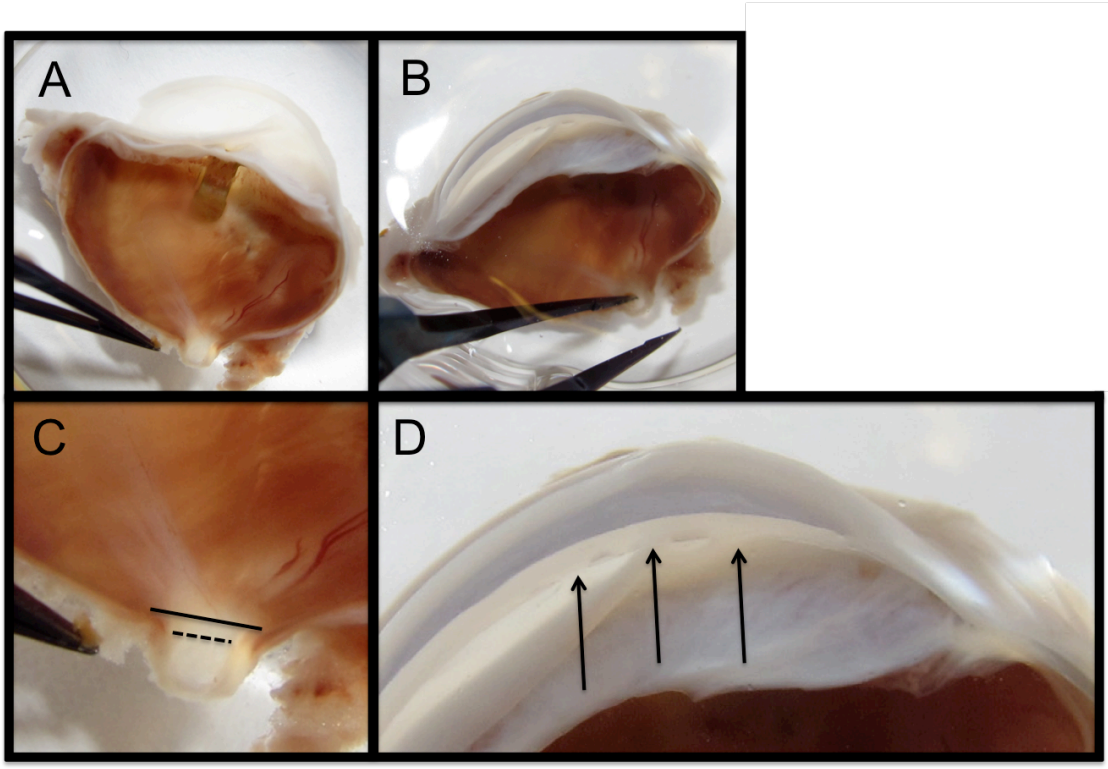

Figure 13. Stereomicroscopy for GS animal with elevated intraocular pressure. Optic disc cupping (A, enlarged in C; solid line - disc, dotted line - cup) and peripheral anterior synechiae (B, enlarged in D; arrows - synechiae).

Light Microscopy

Histologically, both GS and PS were in the suprachoroidal space **(Figure 14)**. One animal implanted with PS was found histologically to have the device in the subretinal space. Histology for this animal showed a retinal scar with retina adherent to the choroid in an area devoid of retinal pigment epithelium **(Figure 15A, B)**. All eyes were devoid of foreign body reaction. Fibrosis was thicker on the scleral side than the choroidal side of the device **(Figure 16C)**, and its presence was confirmed using a Masson's trichrome stain **(Figure 16A, B)**. Generally, fibrosis was more dense at the posterior tail of the device **(Figure 17B)**, and was less compact but thicker toward the anterior end of the device **(Figure 17C)**. GS eyes showed histiocytic inflammation,

which was not found in any GS eyes which received MMC or those implanted with PS **(Figure 16D)**.

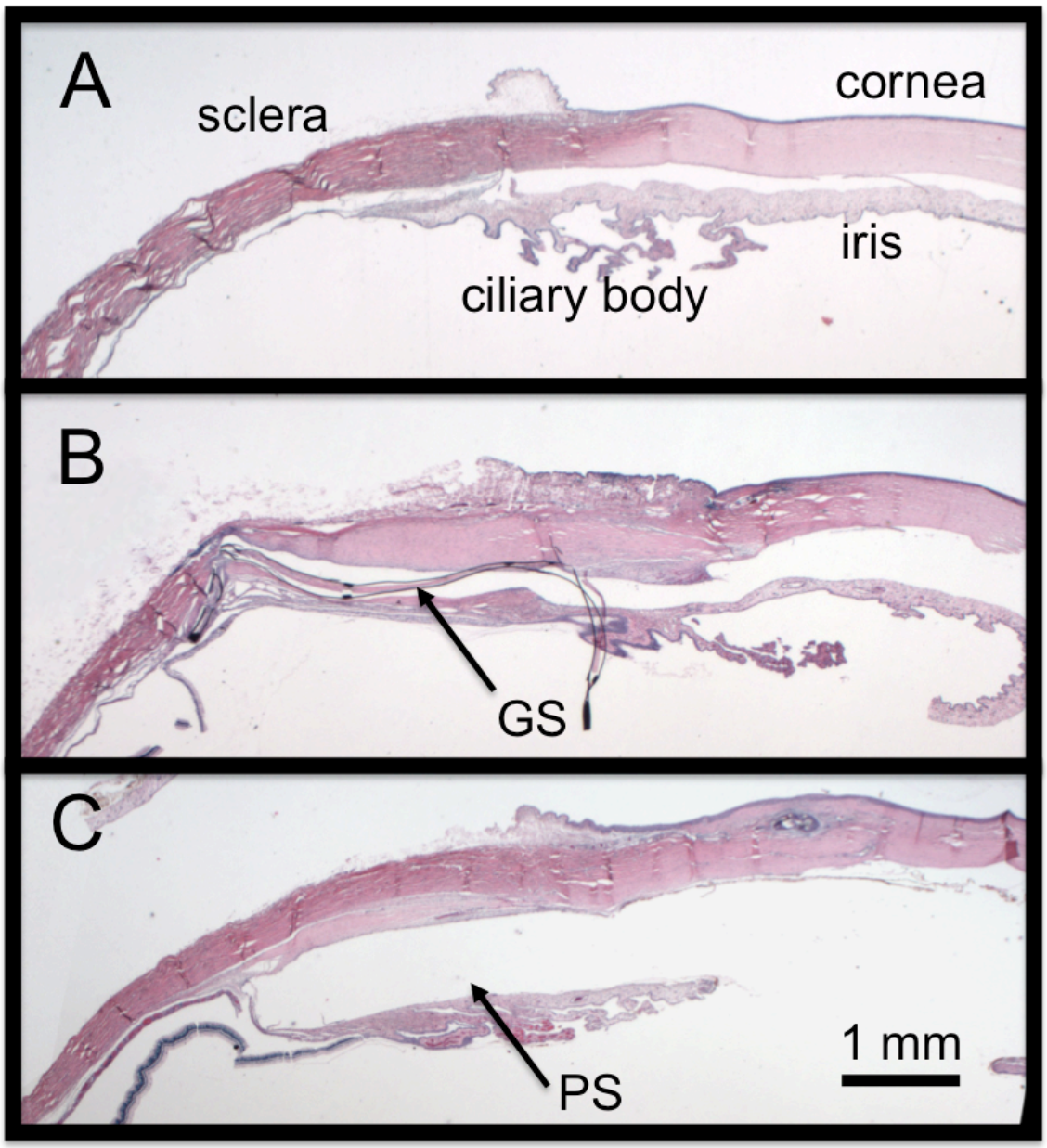

Figure 14. H&E histology slide showing correct device placement of the GS (B) and PS (C) as compared to a control eye with anatomy annotated (A). 1X Magnification.

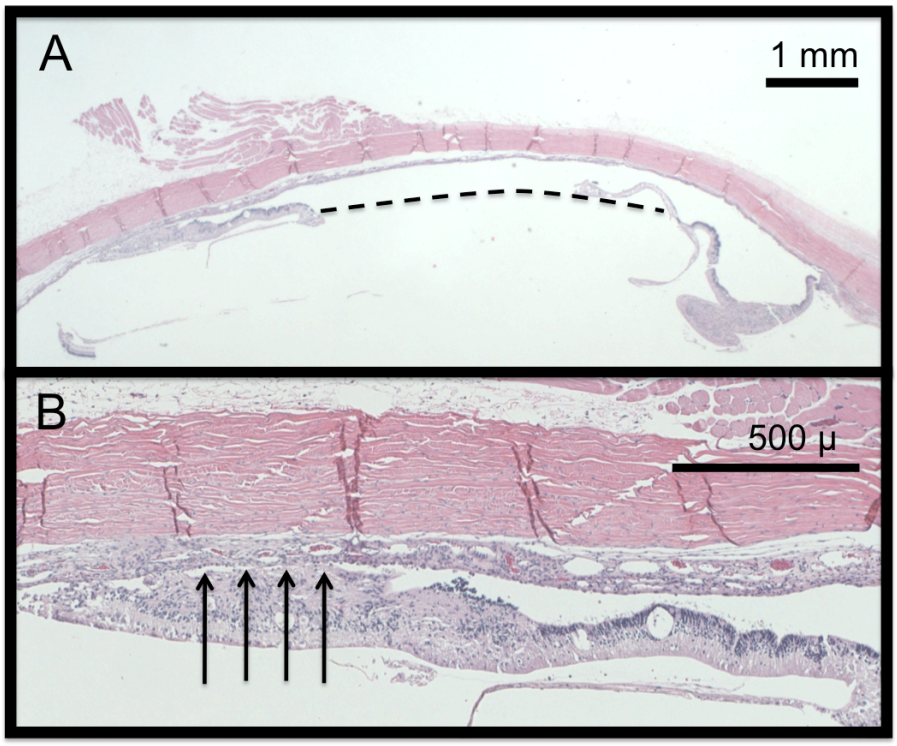

Figure 15. 1X and 4X magnification of same H&E slide - animal with PS placed in the subretinal space, as evidenced by disrupted retina (dotted line) as well as retinal scar (arrows).

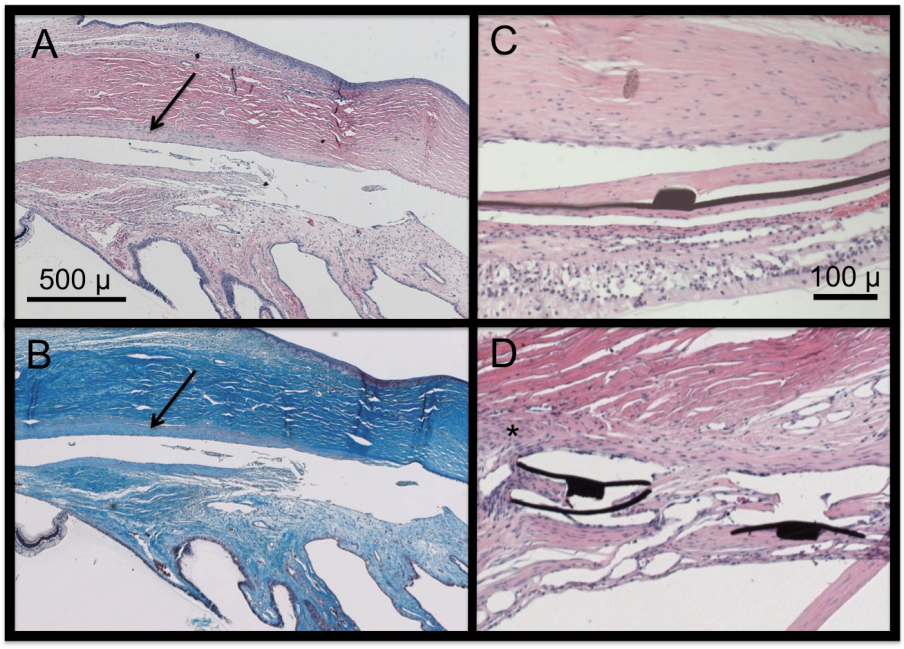

Figure 16. Fibrosis surrounding GS. A, B 4X magnification showing correlation between fibrosis seen on H&E (A) and Masson's trichrome (B). C, D 10X magnification H&E slides showing a thicker layer of fibrosis on scleral side of device versus choroidal (C) and histiocytic inflammation surrounding device (asterisk, D).

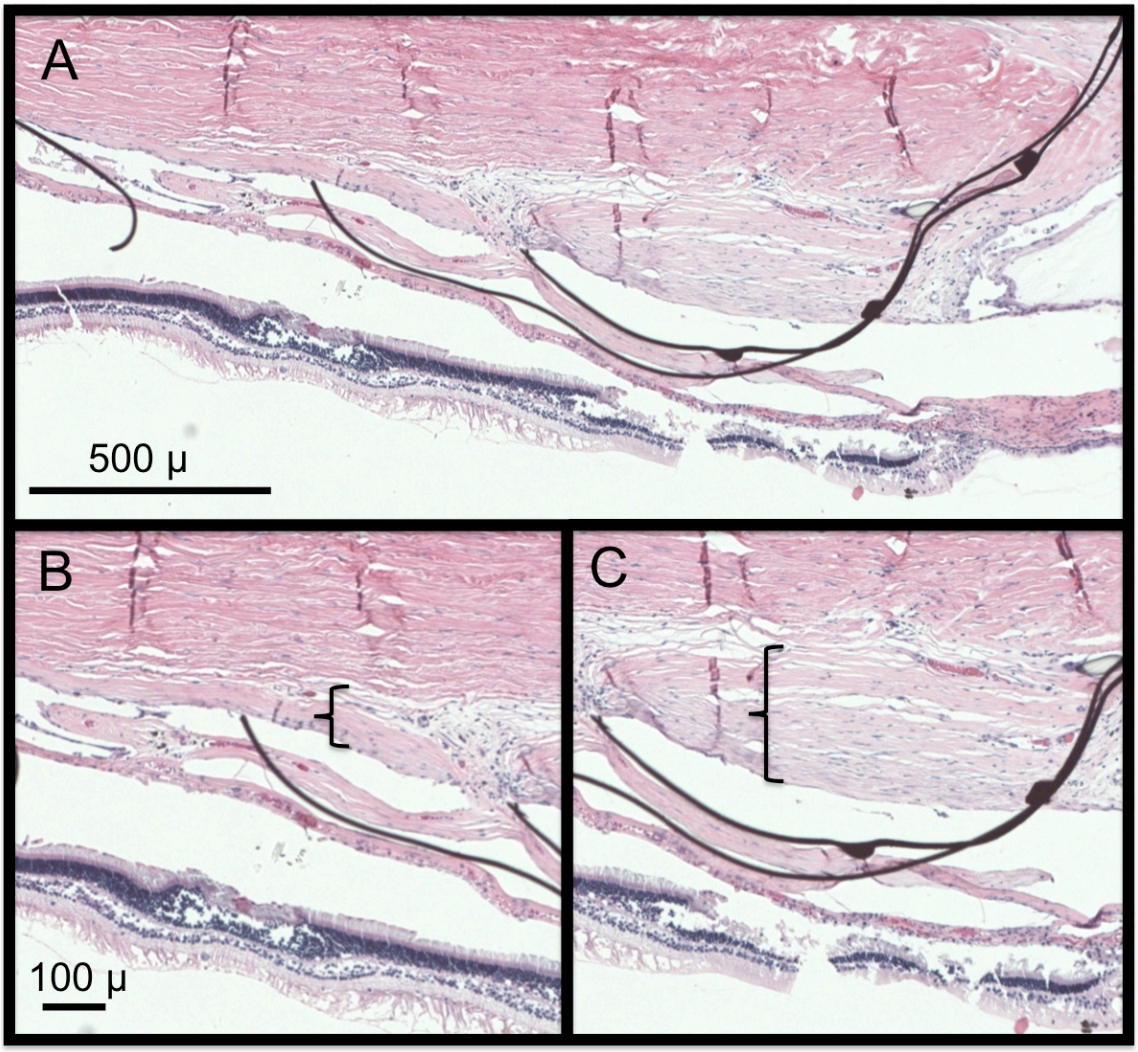

Figure 17. 4X (A) and 10X (B, C) magnification of H&E slide of GS-implanted eye demonstrating the differential in density of fibrosis, more dense toward the posterior end of the device (B) when compared to the more anterior portion (C).

In all animals implanted with GS, regardless of the addition of antimetabolites, fibrosis grew around the device and into the ports, filling the drainage area **(Figure 18A)**. The fibrosis within the device in one animal which did not receive antifibrotics was extensive enough that a discrete vascular structure was observed **(Figure 18B)**. While the PS does not have ports for fibrosis to grow into, one animal exhibited a downgrowth of fibrosis into the space where the device was **(Figure 19)**.

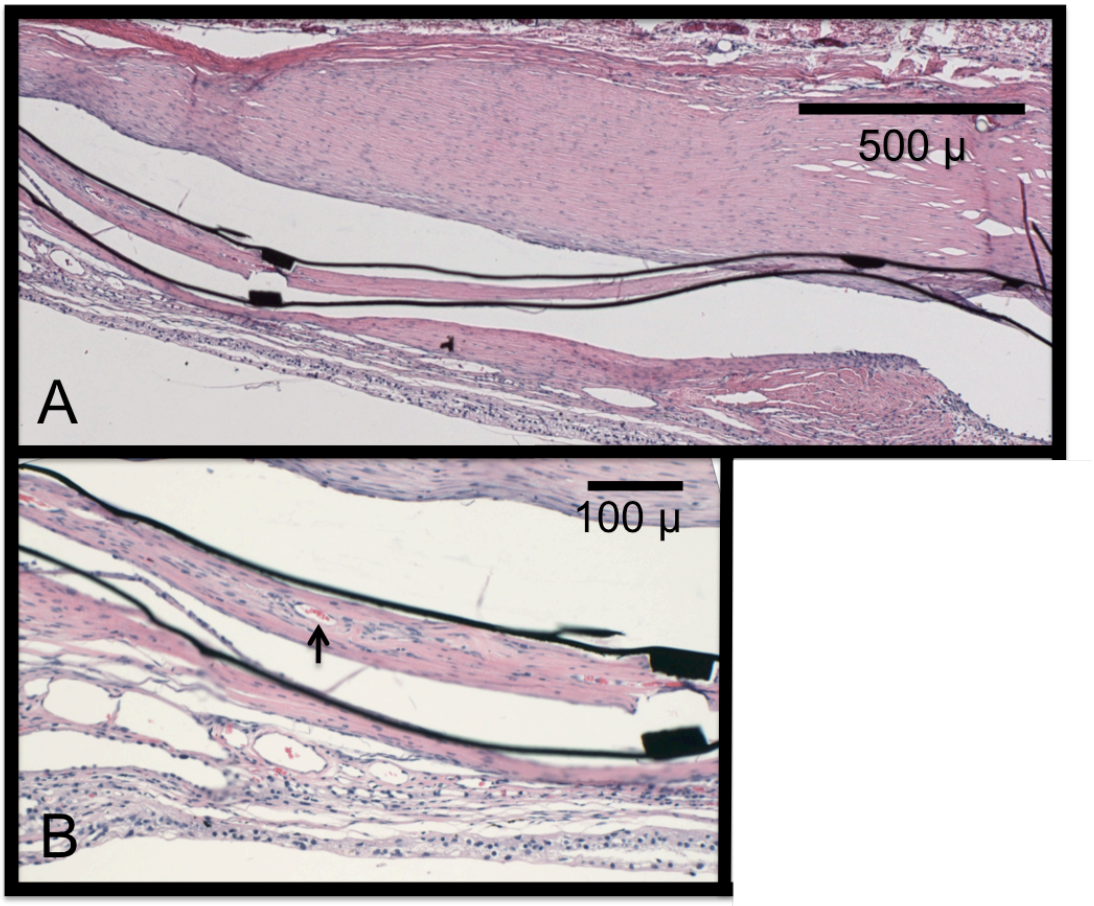

Figure 18. 4X (A) and 10X (B) magnification of H&E slide showing dense fibrosis filling drainage area of GS. Fibrovascular tissues with blood-carrying vessels (arrow, B).

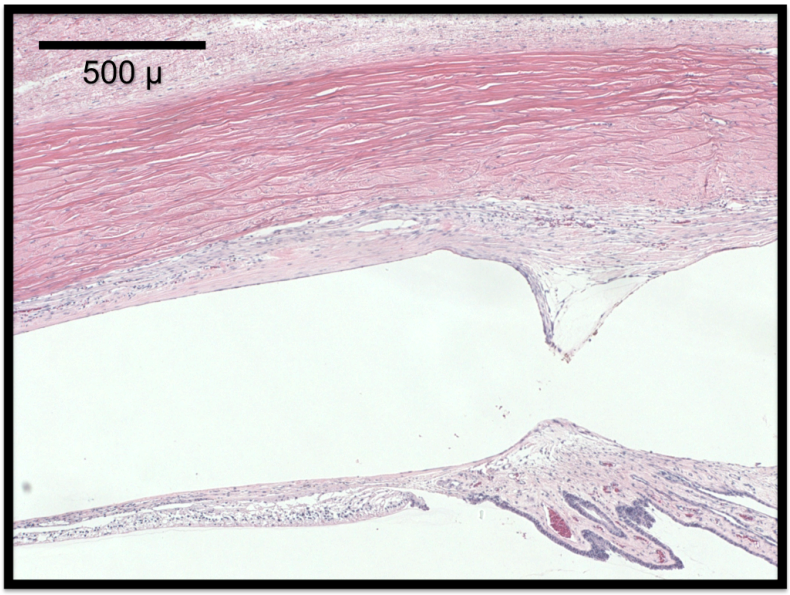

Figure 19. 4X magnification of H&E slide demonstrating downgrowth of fibrosis surrounding PS device.

Histology for the GS-implanted animal with a persistent bleb through week 6 and an unexplained IOP increase showed a closed anterior chamber angle, with iris adherent to cornea in multiple places **(Figure 20)**.

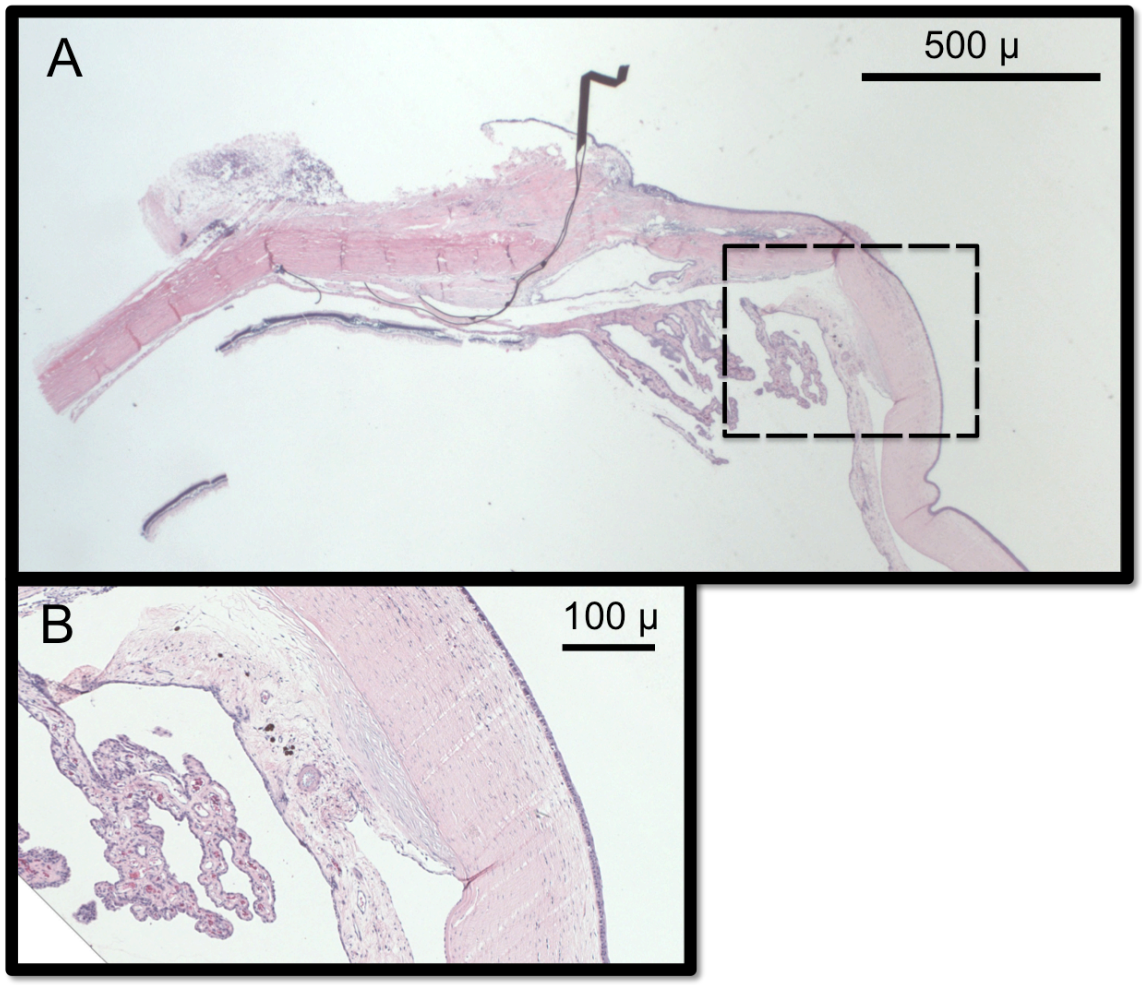

Figure 20. 4X (A) and 10X (B) magnification of H&E slide from GS-implanted animal with unexplained intraocular pressure increase beginning 6 weeks postoperatively. Iridocorneal adhesion visible in the anterior chamber.

Specimens showed a chronic lymphocytic inflammatory response to corneal sutures **(Figure 21)**, which was found adjacent only to sutures, and none of the devices.

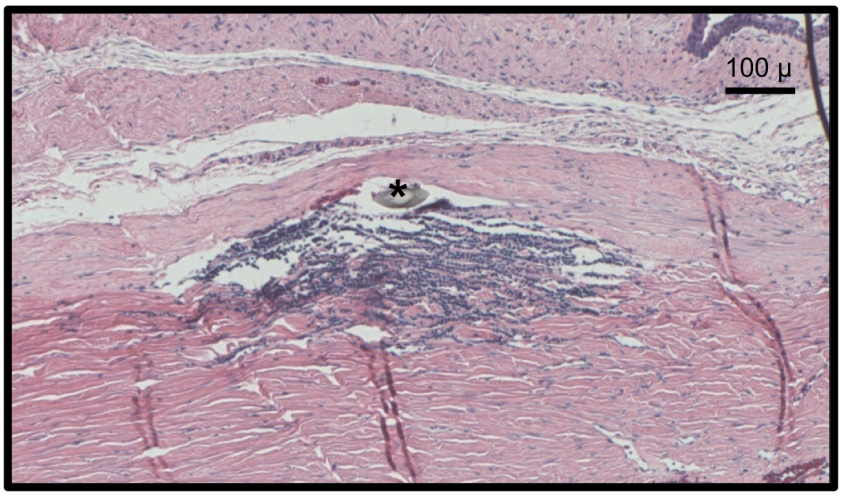

Figure 21. 10X magnification of H&E slide showing lymphocytic inflammation surrounding a suture (asterisk).

Fibrosis Quantification

In all animals implanted with GS, regardless of the addition of antimetabolites, fibrovascular tissue was seen growing into the pores of the device and was present within its lumen **(Figure 18)**. At 15 weeks postoperatively, the thickness of the new fibrosis on the scleral side of the shunt was greater in GS (246 ± 47 µ) and PS (188 ± 47 µ, p=0.285) compared with GS+MMC (109 ± 26 µ, p=0.023 to GS) and PS+MMC (48 ± 30 µ, p=0.028 to PS), respectively **(Figure 22)**. **Figure 23** shows representative histologic sections from each group.

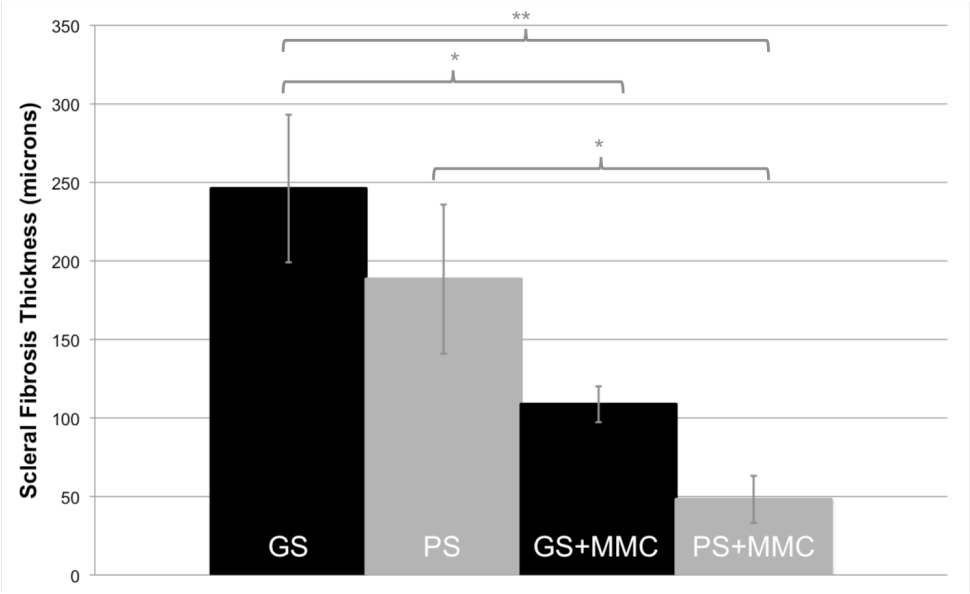

Figure 22. Thickness of scleral fibrosis in all groups 15 weeks postoperatively. Mean ± SEM. * P<.05, ** P<.01.

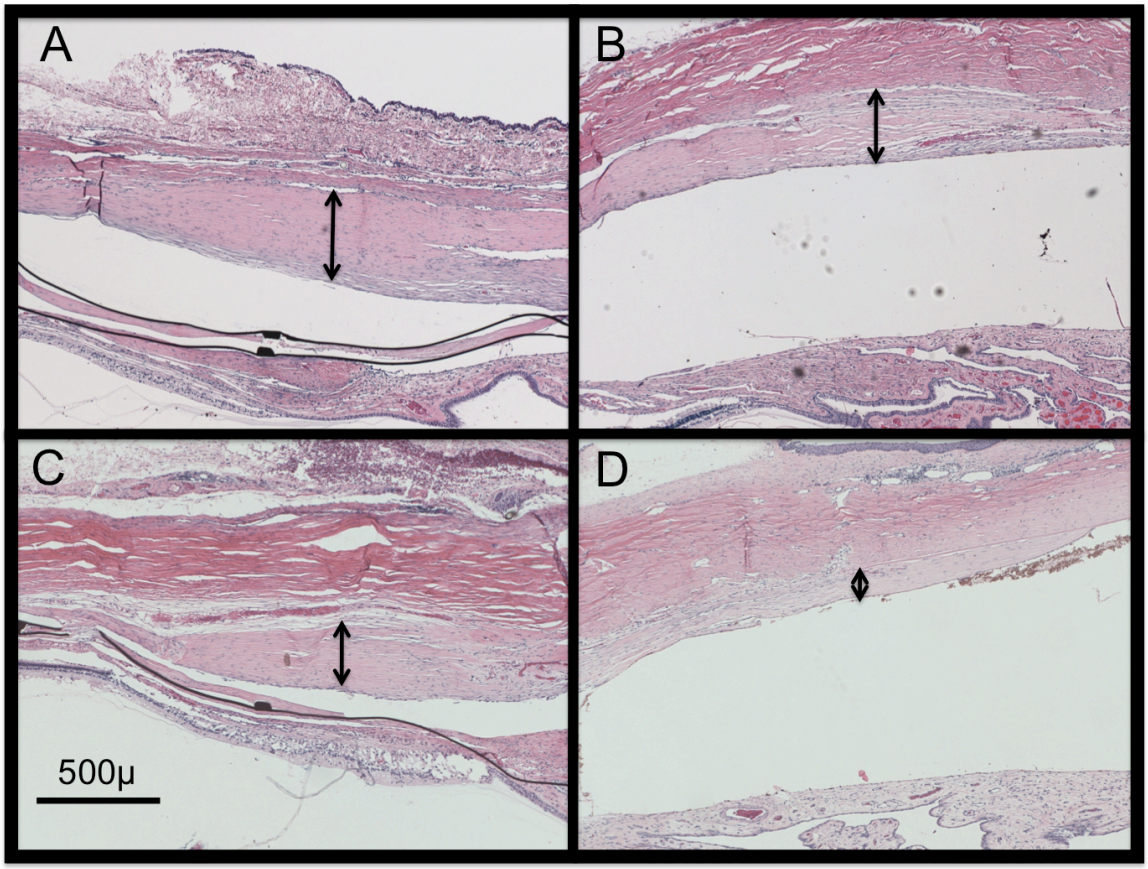

Figure 23. Representative histologic sections from GS (A), PS (B), GS+MMC (C), and PS+MMC (D), 4x magnification. Double-headed arrows represent thickness of fibrosis on scleral side of device.

Overall, the thickness of the fibrosis on the choroidal side of the shunt was much less in all groups (range 17-22 microns), and there was no statistically significant difference between groups at 15 weeks postoperatively **(Figure 24)**.

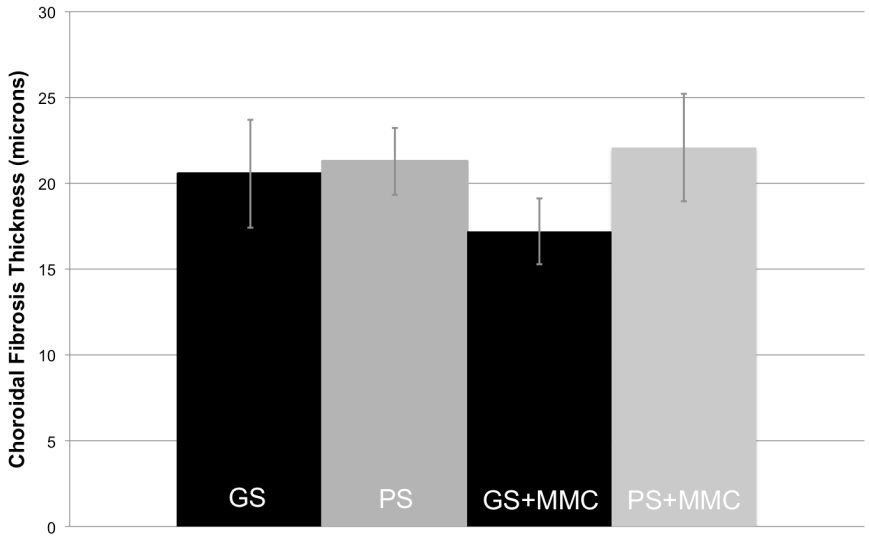

Figure 24. Thickness of choroidal fibrosis 3 months postoperatively. Mean ± SEM.

Ferritin Outflow Tracer

The ferritin outflow tracer was seen surrounding both PS and GS in the suprachoroidal space, including at the tail end of devices filled with fibrovascular tissue **(Figure 25B)**. GS specimens showed thin-walled, large vascular structures within the device **(Figure 25, inset)**.

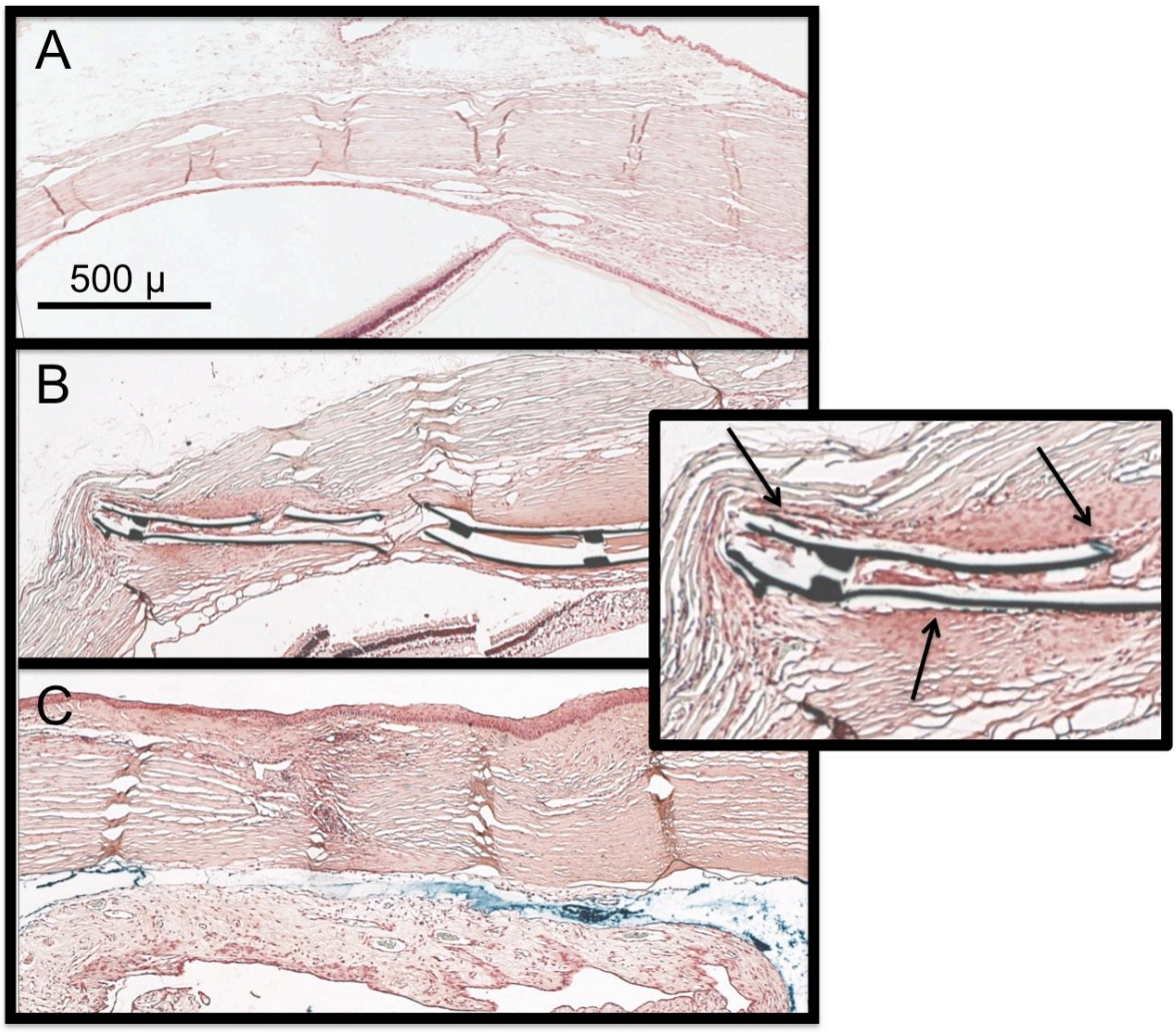

Figure 25. 4X magnification Prussian Blue stain of control eye (A), GS-implanted eye (B), and PS-implanted eye (C) showing ferritin tracer in the suprachoroidal space in device-implanted eyes (blue). PS dissolved in processing and the space collapsed (C). Inset highlighting iron surrounding GS (arrows). Thin-walled, large vascular structures may resemble lymphatic vessels more than blood vessels (inset).

2. Shunt Effect on Intraocular Pressure and Aqueous Humor Dynamics

Pneumatonographic Intraocular Pressure (IOP)

Following acclimatization, rabbits displayed a preoperative diurnal IOP variation, with pressure highest in the evening and lowest in the morning, as has been previously

reported **(Figure 26)**.[30] Average morning IOP was 23.7 ± 2 mm Hg at 0800, and evening IOP was 26.5 ± 2 mm Hg at 2000. (p=0.000).

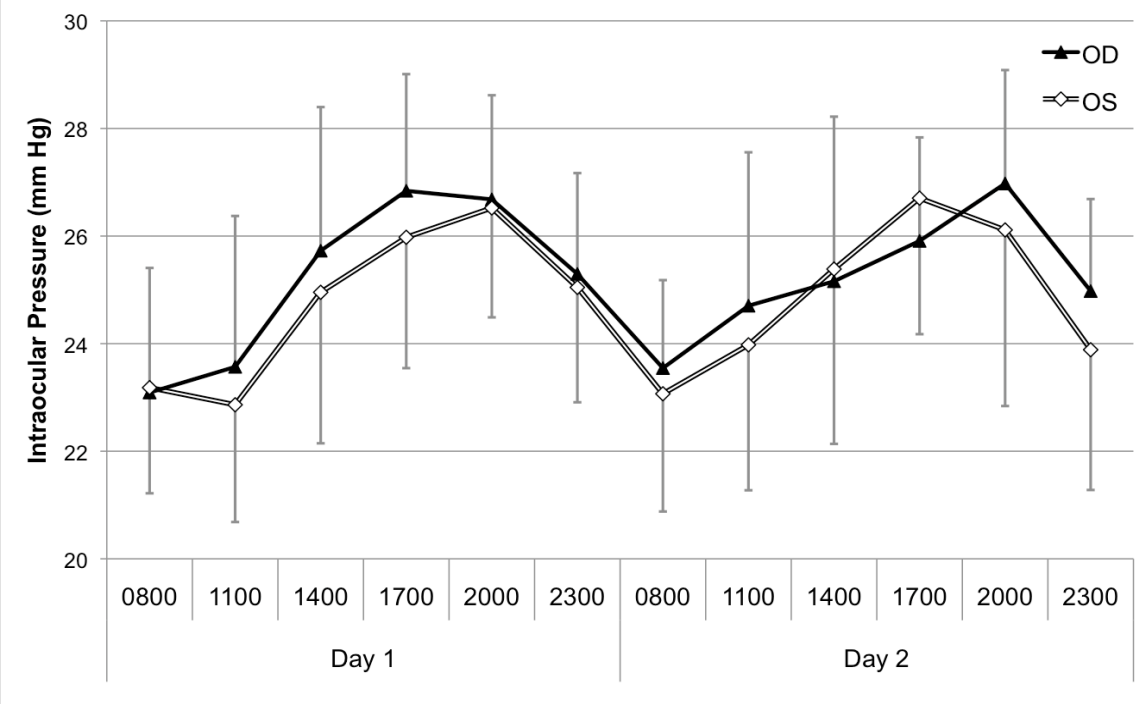

Figure 26. Preoperative diurnal intraocular pressure variation.

Compared to control eyes, all groups showed a consistent decrease in both morning and evening IOP through postoperative week 4 ($p<0.05$). The exception to this was the GS group, which was greater than control eyes at week 1 (control morning, 20.6 ± 3 mm Hg; control evening 24.9 ± 3 mm Hg; GS morning, 21.9 ± 4 mm Hg, p=0.415; GS evening, 25.9 ± 2 mm Hg, p=0.534) **(Figure 27)**. At 15 weeks postoperatively, IOP was lowest in the PS group (morning, 13.7 ± 4 mm Hg, evening 22.7 ± 3 mm Hg) and highest in the GS+MMC group (morning, 21.6 ± 3 mm Hg, evening 29.9 ± 5 mm Hg), both values greater than control eyes. Evening IOP showed a more gradual return to baseline pressure through postoperative 15 weeks as compared to morning IOP **(Figure 27)**.

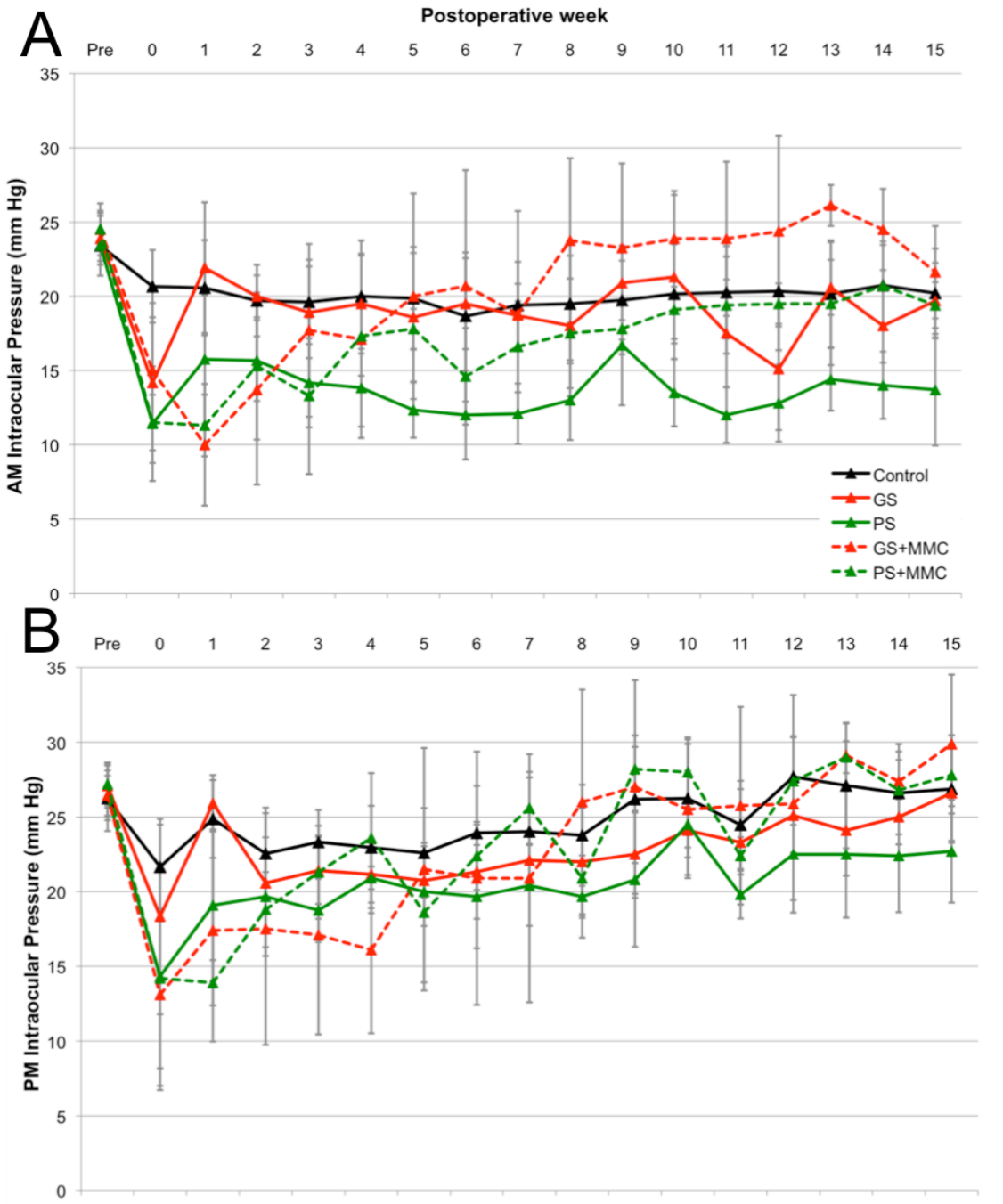

Figure 27. Absolute intraocular pressure (IOP) through 15 weeks postoperatively, morning (A) and evening (B).

Morning IOP was decreased from baseline through 15 weeks postoperatively in all groups (Control 15%; GS 18%; GS+MMC 14%; PS 41%; PS+MMC 21%); however,

this was only statistically significant as compared to control eyes in the PS group through 15 weeks, the PS+MMC group through 7 weeks, and the GS+MMC group through 3 weeks. Evening IOP was decreased through 8 weeks postoperatively (Control 9%; GS 19%; GS+MMC 1%; PS 27%; PS+MCC 23%). Compared to control eyes, this decrease was significant in both MMC groups through 4 weeks, through 15 weeks in the PS group, and non-significant in the GS group **(Table 2, 3)**.

Table 2. AM Percent IOP decrease through postoperative week 15.

	CONTROL	GS		PS		GS+MMC		PS+MMC					
Postop week	% change	% change	p*	% change	p*	% change	p*	% change	p*	p**	p***	p****	p******
0	-12.47% ±14%	-37.14% ±24%	0.000	-53.49% ±18%	0.000	-40.11% ±17%	0.001	-53.14% ±7%	0.000	0.225	0.863	0.804	0.134
1	-12.19% ±17%	-3.72% ±13%	0.690	-36.05% ±19%	0.008	-56.75% ±16%	0.000	-53.67% ±10%	0.000	0.015	0.000	0.038	0.576
2	-17.71% ±10%	-17.45% ±5%	0.927	-35.55% ±13%	0.011	-37.23% ±21%	0.000	-37.89% ±19%	0.002	0.045	0.002	0.538	0.437
3	-16.88% ±10%	-21.57% ±14%	0.482	-42.11% ±13%	0.001	-21.58% ±15%	0.076	-46.22% ±20%	0.000	0.026	0.346	0.409	0.052
4	-15.97% ±12%	-17.59% ±13%	0.509	-42.84% ±13%	0.000	-25.52% ±24%	0.020	-29.53% ±10%	0.032	0.009	0.150	0.200	0.880
5	-16.68% ±12%	-20.64% ±16%	0.257	-47.57% ±8%	0.000	-10.82% ±16%	0.523	-27.32% ±7%	0.085	0.004	0.729	0.023	0.384
6	-19.68% ±18%	-15.58% ±11%	0.505	-47.33% ±17%	0.003	-6.89% ±19%	0.708	-40.67% ±12%	0.041	0.005	0.895	0.481	0.038
7	-18.40% ±11%	-22.68% ±9%	0.803	-48.92% ±11%	0.001	-16.71% ±21%	0.321	-32.53% ±11%	0.032	0.004	0.854	0.066	0.343
8	-17.39% ±16%	-25.19% ±21%	0.770	-43.57% ±13%	0.030	-6.10% ±18%	0.200	-28.57% ±15%	0.173	0.054	0.082	0.110	0.042
9	-16.58% ±11%	-13.27% ±14%	0.680	-28.16% ±20%	0.274	-7.87% 20%	0.256	-27.41% ±7%	0.103	0.094	0.560	0.932	0.041
10	-15.06% ±12%	-11.02% ±28%	0.520	-42.32% ±10%	0.046	-5.10% 11%	0.215	-22.11% 8%	0.334	0.002	0.542	0.033	0.086
11	-14.41% ±12%	-27.69% ±15%	0.133	-48.94% ±6%	0.001	-5.43% 18%	0.207	-21.06% 12%	0.304	0.012	0.013	0.001	0.075
12	-14.30% ±15%	-38.20% ±14%	0.057	-45.39% ±11%	0.015	-3.39% 24%	0.196	-20.23% 9%	0.438	0.455	0.002	0.012	0.104
13	-14.91% ±14%	-14.62% ±11%	0.709	-38.31% ±11%	0.042	4.10% 6%	0.017	-20.13% 19%	0.454	0.010	0.050	0.044	0.013
14	-12.38% ±12%	-25.27% ±13%	0.317	-40.05% ±11%	0.012	-2.63% 8%	0.130	-15.75% 10%	0.561	0.049	0.006	0.002	0.096
15	-14.75% ±11%	-18.03% ±15%	0.944	-41.25% ±17%	0.005	-14.10% 10%	0.921	-20.98% 5%	0.308	0.004	0.627	0.011	0.397

p* compared to control eyes; p** GS to PS; p*** GS to GS+MMC; p**** PS to PS+MMC; p*****GS+MMC to PS+MMC

Table 3. PM Percent IOP decrease from baseline through postoperative week 15.

	CONTROL	GS		PS		GS+MMC		PS+MMC					
Postop week	% change	% change	p*	% change	p*	% change	p*	% change	p*	p**	p***	p****	p******
0	-16.36% ± 16%	-23.83% ± 21%	0.137	-43.35% ± 32%	0.005	-47.13% ± 21%	0.003	-47.03% ± 30%	0.006	0.259	0.149	0.902	0.806
1	-5.73% ± 8%	-5.99% ± 7%	0.923	-29.84% ± 21%	0.002	-24.82% ± 23%	0.000	-48.59% ± 8%	0.000	0.010	0.002	0.026	0.130
2	-14.11% ± 11%	-24.49% ± 8%	0.125	-25.79% ± 18%	0.083	-24.63% ± 24%	0.006	-30.64% ± 11%	0.020	0.868	0.252	0.530	0.726
3	-11.08% ± 6%	-22.43% ± 4%	0.055	-28.46% ± 11%	0.001	-26.33% ± 18%	0.000	-21.34% ± 13%	0.066	0.237	0.043	0.275	0.057
4	-12.25% ± 8%	-22.36% ± 7%	0.068	-19.91% ± 10%	0.109	-29.34% ± 8%	0.000	-13.36% ± 15%	0.877	0.852	0.015	0.270	0.001
5	-14.64% ± 11%	-20.09% ± 2%	0.158	-25.46% ± 10%	0.126	-5.51% ± 15%	0.547	-31.51% ± 18%	0.017	0.921	0.555	0.403	0.149
6	-8.03% ± 10%	-17.62% ± 6%	0.018	-26.35% ± 15%	0.005	-8.41% ± 21%	0.106	-17.57% ± 9%	0.248	0.607	0.925	0.363	0.753
7	-8.82% ± 10%	-17.88% ± 3%	0.376	-22.36% ± 10%	0.039	-8.50% ± 19%	0.092	-5.84% ± 8%	0.067	0.554	0.762	0.045	0.095
8	-8.94% ± 13%	-18.53% ± 10%	0.019	-27.04% ± 11%	0.007	-0.54% ± 25%	0.283	-22.69% ± 13%	0.069	0.417	0.062	0.745	0.023
9	-0.16% ± 13%	-16.33% ± 9%	0.286	-20.92% ± 15%	0.069	3.33% 24%	0.649	3.72% ± 3%	0.064	0.603	0.041	0.008	0.966
10	-0.13% ± 11%	-10.18% ± 7%	0.269	-6.77% ± 11%	0.145	-2.00% 14%	0.748	3.06% 9%	0.548	0.611	0.253	0.148	0.477
11	-6.25% ± 12%	-13.73% ± 8%	0.025	-24.27% ± 9%	0.005	-1.46% 22%	0.465	-17.43% 7%	0.068	0.167	0.130	0.366	0.052
12	6.05% ± 11%	-6.66% ± 8%	0.085	-14.31% ± 10%	0.006	-0.96% 25%	0.325	0.94% 12%	0.432	0.350	0.511	0.068	0.825
13	3.36% ± 14%	-10.60% ± 8%	0.261	-14.31% ± 15%	0.087	12.25% 5%	0.189	6.74% 4%	0.581	0.630	0.008	0.009	0.501
14	1.61% ± 8%	-7.08% ± 4%	0.373	-14.57% ± 14%	0.006	5.54% 8%	0.416	-1.26% 9%	0.513	0.181	0.037	0.021	0.250
15	2.23% ± 8%	-1.36% ± 7%	0.799	-13.31% ± 14%	0.034	14.99% 15%	0.025	2.42% 9%	0.971	0.065	0.019	0.017	0.067

p* compared to control eyes; p** GS to PS; p*** GS to GS+MMC; p**** PS to PS+MMC; p*****GS+MMC to PS+MMC

Aqueous Flow and Tonographic Outflow Facility

There was no difference in aqueous flow (F_a) between groups preoperatively, with an average of 3.3 ± .7 µL/min. Compared to the unoperated eyes, F_a was not different in shunt eyes at any time point. Average preoperative tonographic outflow facility (C_t) was 0.31 ± 0.09 µL/min/mm Hg. The only significant difference was found at 3 months, when both groups receiving antimetabolites exhibited greater C_t than control groups (control, 0.34 ± 0.16 µL/min/mm Hg; GS+MMC, 0.56 ± 0.13 µL/min/mm Hg, p=0.007; PS+MMC, 0.48 ± 0.14 µL/min/mm Hg, p=0.049) **(Figure 28)**.

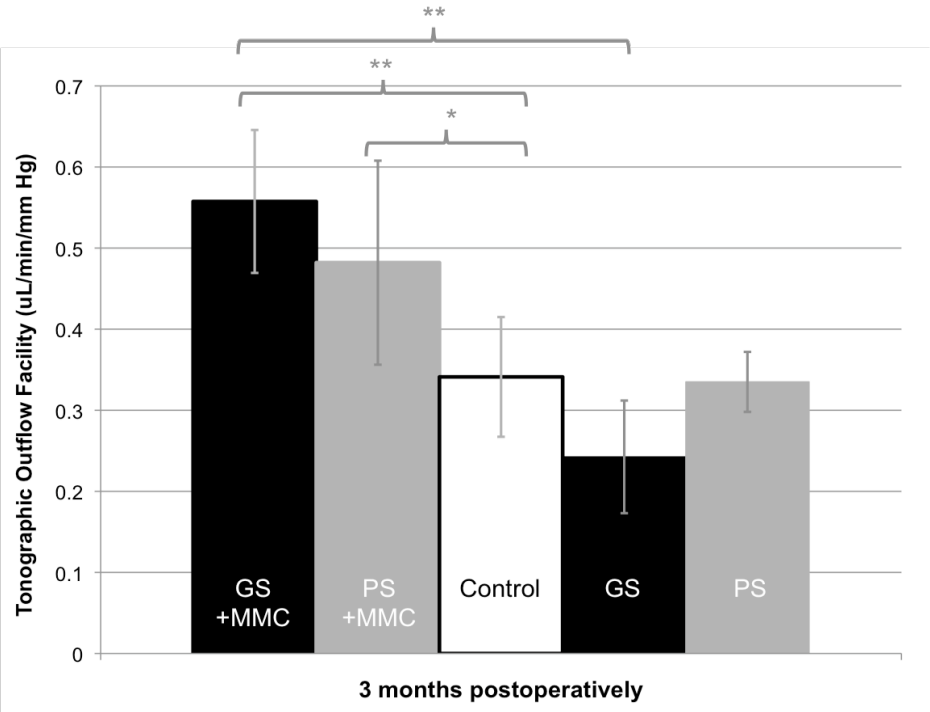

Figure 28. Tonographic outflow facility (C_t) in all groups at 3 months postoperatively. * P < .05, ** P < .01.

Tonographic Uveoscleral Flow

Average preoperative tonographic uveoscleral flow (F_{ut}) was 2.02 ± 1.30 µL/min. At 3 months postoperatively, GS+MMC and PS+MMC exhibited a small but significant decline compared to GS (GS+MMC, p=0.017; PS+MMC, p=0.033) and PS (GS+MMC, p=0.001; PS+MMC, p=0.002).

Fluorophotometric Outflow Facility

Overall average preoperative fluorophotometric outflow facility (C_f) was 0.18 ± .5 µL/min/mm Hg. Standard deviations in the intervention groups through postoperative 3 months were large, obscuring patterns of changes in C_f. No statistically significant difference could be detected. Average preoperative fluorophotometric uveoscleral flow

(F_{uf}) was 1.35 ± 5.71 μL/min. There was no statistically significant change in F_{uf} through 3 months in any group, and no differences between groups at 3 months postoperatively.

DISCUSSION

This is the first study to systematically compare different suprachoroidal shunts and shunt materials both in vitro and in vivo. Fibrosis and foreign body reaction in the suprachoroidal space have not been formally examined. The idea of lowering IOP by creating a cyclodialysis cleft was first realized at the beginning of the 20th century,[31] but complicated by unpredictable closure of the cleft responsible for aqueous humor drainage. Extended function seemed possible with cleft maintainers;[32] however, materials available at that time were not tolerated well enough. Advances in engineering and material sciences have now allowed the reduction of bioreactivity and internal drainage device size. We chose rabbits for this study to allow the rapid wound healing and fibrosis in this species to display differences in biocompatibility and shunt function within only a few weeks, as classic glaucoma surgery in albino rabbits in the form of trabeculectomy tends to fail within several days.[33] Also, rabbits normally have limited uveoscleral outflow,[34] therefore, enhancing drainage into this space may be more noticeable.

Before establishing a suprachoroidal shunt fibrosis model in vivo, we first assessed in vitro growth patterns of cell types that are expected to come into contact with suprachoroidal shunts. We then compared two different shunt materials to distinguish basic material effects from additional immune reactivity present in vivo. Because neither shunt was sufficiently translucent, we developed a reflection-based fluorescent assay with FIV-mediated[16,35] stably eGFP-expressing cell lines of fibroblast, trabecular meshwork, and endothelial origin. Our assay allowed cell counts and direct observation of growth

patterns.

As a chemically non-reactive precious metal, gold has been hypothesized to have ideal features that are strikingly different from conventional shunt materials: gold surfaces can be manufactured to be devoid of nano-structures which encourage cell migration and differentiation.[36-39] However, for intraocular use, pure elemental gold has to be used to avoid traces of toxic copper,[40] and the low hardness[41] poses considerable engineering challenges to allow handling during surgery. The GS used here was produced with photolithographic etching to provide increased resistance to torque provided by internal pillars instead of grooves. In contrast, the polypropylene of the PS shunt is a thermoplastic polymer that can be melt-processed by extrusion and molding and is inert yet flexible and inexpensive. When observed under an electron microscope, polypropylene is uneven and has pico- and nano-scale grooves.[42] Despite these distinct material differences, the cell growth patterns we observed were unchanged on GS or PS.

Both preoperatively and postoperatively, animals exhibited the known 24 hour IOP pattern,[30] validating our measurements. Because IOP increases slightly with age in young rabbits,[22] right eye to left eye comparison was preferable here over same eye comparison. Pneumatonometry is often used in clinical research for circadian IOP measurements.[43-45] Tonopen consistently underestimates IOP with increasing inaccuracy at higher pressures, but is also fast and simple.[46-48] Both have been used in the rabbit before[46,47,49] but this is the first systematic comparison in a glaucoma procedure study that may alter flow and displaceability of aqueous humor. The IOP difference of approximately 50% between these two was striking and most likely primarily the result of a CCT that is only about 60% of that in a human eye.[50]

The length of IOP reduction with both GS and PS was considerably longer than is

achievable by any other glaucoma surgery in this species which is often limited to days or weeks.[29,33,51] In our right to left eye comparison, GS lowered IOP significantly primarily in the PM from postoperative weeks 6 through 11. In contrast, PS resulted in significantly lower IOP more often in the AM than in the PM. This might well be caused by the difference with which these devices gain access to outflow routes and how they contribute to IOP during different times of the day. GS might have developed a different, more fibrovascular access to the pressure-independent uveoscleral outflow as compared to PS that has more classical bleb wall features.

Lower IOP with the PS compared to GS cannot simply be explained by a larger internal diameter and less flow resistance, but may be a direct result of absorption area. Considering that pressure, filtration space, and transmural gradient are related, it is possible that flow through the larger internal space of the PS is relatively less affected by fibrosis than the GS.

Our attempt to extend and enhance device function with adjuvant MMC and TAC caused a marked IOP decrease only during the first 4 weeks with the GS and first 7 weeks with the PS, but was less than in non-MMC animals thereafter. The results for MMC and TAC with conventional glaucoma drainage devices have been similarly sobering[52] possibly because the mechanism is not fibrosis alone but also a foreign body reaction.[53] We did not observe foreign body reaction in our experiments, and other mechanisms could explain a worse long-term IOP in eyes receiving MMC and TAC: as seen in one animal, channels towards the subconjunctival space might have formed in the early postoperative period and prevented the establishment of proper suprachoroidal drainage. Increased tonographic outflow facility in these eyes is consistent with this hypothesis, indicating that aqueous humor was displaceable, possibly through needle

tracks in the presence of reduced wound healing. Increased IOP can then result when the bleb disappears. Additionally, TAC might have worsened trabecular outflow as seen in steroid induced glaucoma,[54] while MMC might have caused avascularity in the area applied,[55] reducing uveoscleral outflow.

The present standard for implantation of both the GS and PS in clinical trials in humans is transscleral insertion, but in the rabbit, such an ab externo approach is highly traumatic due to a thin, friable sclera with firmly adherent uvea. We developed an ab interno insertion technique with well controlled visco-hydraulic expansion of the suprachoroidal space and proper positioning of the shunt to standardize insertion and achieve consistent results. The adjacent corneal thickness was unaffected and maintained a normal diurnal thickness cycle.[22] In attempting to determine the mechanism of IOP reduction by GS and PS, we found that fluorophotometric outflow measurements were not significantly different following the perturbations and considerable standard deviation these surgeries induced.

Consistent with the idea of reduced fibrosis in the suprachoroidal space, fibrosis on the choroidal side of these shunts measured only 20 microns, while that on the scleral side was 200 to 250 microns thick, similar to what occurs with external drainage devices or trabeculectomies in rabbits,[56,57] which is overall similar to[58] or slightly less than[59] that in humans. This striking difference between the two sides may be a direct result of the cell types and quantities adjacent to the shunt. The internal sclera is the same fibroblast-rich structure that external drainage devices are in contact with, while the highly vascularized choroid is detached from the scleral bed and might contain fewer fibroblasts. Similar to our in vitro experiments, no significant differences were seen between GS and PS, although PS was 25% thinner on average. In the absence of significant cellular

inflammation, capsule formation might be a direct result of aqueous humor flow,[60-62] and the 20 times smaller surface area of the GS compared with PS might explain capsule differences. Several GS-implanted eyes displayed considerable ingrowth of a mixed fibrovascular tissue, but this did not prevent the entry of tracer into the device. Vascular profiles identified included some with histologic features of blood vessels (with narrow, normal endothelium and basement membrane, and red blood cells in the lumen) and others more consistent with lymphatic vessels (with thin endothelium, poorly developed basement membrane, and no red blood cells visible). These neo-vessels could represent new structures that provide access to uveoscleral drainage routes. A similar mechanism is deployed in a recently introduced external glaucoma drainage device that utilizes a porous material to encourage ingrowth while conserving other design features.[63] Due to the sparsity of material, we were not able to differentiate between primarily vascular or lymphatic origin by immunohistology.

In summary, the suprachoroidal shunts studied here lowered intraocular pressure up to 7 times longer than classical glaucoma surgery in this species. Fibroblast, trabecular meshwork, and endothelial cell growth indicated similar in vitro biocompatibility. In vivo, fibrosis occurred more on the scleral than on the choroidal side of the shunt and was observed inside the lumen of the gold shunt as well. The larger polypropylene shunt lowered pressure more and longer than the gold shunt, but had more severe complications which were also more frequent. The use of mitomycin C and triamcinolone worsened intraocular pressure response. Tracer experiments demonstrated shunt function up to the experimental endpoint of 15 weeks. In the absence of a significant decrease in aqueous humor production or increased trabecular flow, the main mechanism of intraocular pressure lowering was likely an increase in uveoscleral outflow.

REFERENCES

1. Congdon N, O'Colmain B, Klaver CC, et al. Causes and prevalence of visual impairment among adults in the United States. Arch Ophthalmol 2004;122:477-85.
2. Oeppen J, Vaupel JW. Demography. Broken limits to life expectancy. Science 2002;296:1029-31.
3. Gedde SJ, Heuer DK, Parrish RK, 2nd. Review of results from the Tube Versus Trabeculectomy Study. Curr Opin Ophthalmol 2010;21:123-8.
4. Ramulu PY, Corcoran KJ, Corcoran SL, Robin AL. Utilization of various glaucoma surgeries and procedures in Medicare beneficiaries from 1995 to 2004. Ophthalmology 2007;114:2265-70.
5. Schwartz KS, Lee RK, Gedde SJ. Glaucoma drainage implants: a critical comparison of types. Curr Opin Ophthalmol 2006;17:181-9.
6. Yaldo MK, Stamper RL. Long-term effects of mitomycin on filtering blebs. Lack of fibrovascular proliferative response following severe inflammation. Arch Ophthalmol 1993;111:824-6.
7. Emi K, Pederson JE, Toris CB. Hydrostatic pressure of the suprachoroidal space. Invest Ophthalmol Vis Sci 1989;30:233-8.
8. Francis BA, Singh K, Lin SC, et al. Novel glaucoma procedures: a report by the American Academy of Ophthalmology. Ophthalmology 2011;118:1466-80.
9. Lee PP, Walt JW, Rosenblatt LC, Siegartel LR, Stern LS. Association between intraocular pressure variation and glaucoma progression: data from a United States chart review. Am J Ophthalmol 2007;144:901-7.
10. Caprioli J, Coleman AL. Intraocular pressure fluctuation a risk factor for visual field progression at low intraocular pressures in the advanced glaucoma intervention study. Ophthalmology 2008;115:1123-9 e3.
11. Liu JH, Zhang X, Kripke DF, Weinreb RN. Twenty-four-hour intraocular pressure pattern associated with early glaucomatous changes. Invest Ophthalmol Vis Sci 2003;44:1586-90.
12. David R, Zangwill L, Briscoe D, Dagan M, Yagev R, Yassur Y. Diurnal intraocular pressure variations: an analysis of 690 diurnal curves. Br J Ophthalmol 1992;76:280-3.
13. Loewen NA, Liu JH, Weinreb RN. Increased 24-hour variation of human intraocular pressure with short axial length. Invest Ophthalmol Vis Sci 2010;51:933-7.
14. Bagga H, Liu JH, Weinreb RN. Intraocular pressure measurements throughout the 24 h. Curr Opin Ophthalmol 2009;20:79-83.
15. Weinreb RN, Toris CB, Gabelt BT, Lindsey JD, Kaufman PL. Effects of prostaglandins on the aqueous humor outflow pathways. Surv Ophthalmol 2002;47 Suppl 1:S53-64.
16. Loewen N, Fautsch MP, Teo WL, Bahler CK, Johnson DH, Poeschla EM. Long-term, targeted genetic modification of the aqueous humor outflow tract coupled with noninvasive imaging of gene expression in vivo. Invest Ophthalmol Vis Sci 2004;45:3091-8.

17. Khare PD, Loewen N, Teo W, et al. Durable, safe, multi-gene lentiviral vector expression in feline trabecular meshwork. Mol Ther 2008;16:97-106.
18. Barraza RA, Rasmussen CA, Loewen N, et al. Prolonged transgene expression with lentiviral vectors in the aqueous humor outflow pathway of nonhuman primates. Hum Gene Ther 2009;20:191-200.
19. Saenz DT, Barraza R, Loewen N, Teo W, Poeschla EM. Feline immunodeficiency virus-based lentiviral vectors. Cold Spring Harb Protoc 2012;2012:71-6.
20. Saenz DT, Barraza R, Loewen N, Teo W, Poeschla EM. Titration of feline immunodeficiency virus-based lentiviral vector preparations. Cold Spring Harb Protoc 2012;2012:126-8.
21. Saenz DT, Barraza R, Loewen N, Teo W, Poeschla EM. Production and harvest of feline immunodeficiency virus-based lentiviral vector from cells grown in T75 tissue-culture flasks. Cold Spring Harb Protoc 2012;2012:124-5.
22. Zhao M, Hejkal JJ, Camras CB, Toris CB. Aqueous humor dynamics during the day and night in juvenile and adult rabbits. Invest Ophthalmol Vis Sci 2010;51:3145-51.
23. Toris CB, Yablonski ME, Wang YL, Hayashi M. Prostaglandin A2 increases uveoscleral outflow and trabecular outflow facility in the cat. Exp Eye Res 1995;61:649-57.
24. Toris CB, Zhan GL, Yablonski ME, Camras CB. Effects on aqueous flow of dorzolamide combined with either timolol or acetazolamide. J Glaucoma 2004;13:210-5.
25. Yablonski ME, Hayashi M, Cook DJ, Chubak G, Sirota M. Fluorophotometric study of intravenous carbonic anhydrase inhibitors in rabbits. Invest Ophthalmol Vis Sci 1987;28:2076-82.
26. Liu CJ, Cheng CY, Ko YC, Lau LI. Determinants of Long-term Intraocular Pressure After Phacoemulsification in Primary Angle-closure Glaucoma. J Glaucoma 2011.
27. Langham ME, Edwards N. A new procedure for the measurement of the outflow facility in conscious rabbits. Exp Eye Res 1987;45:665-72.
28. Zamora DO, Kiel JW. Topical proparacaine and episcleral venous pressure in the rabbit. Invest Ophthalmol Vis Sci 2009;50:2949-52.
29. Lei J, Sun N, Zhao X, Kang Q, Chen L, Fan X. Morphologic study of the drainage pathway using a tracer after a bypass filtering procedure in rabbit eyes. Ophthalmic Surg Lasers Imaging 2011;42:254-62.
30. Bar-Ilan A. Diurnal and seasonal variations in intraocular pressure in the rabbit. Exp Eye Res 1984;39:175-81.
31. Fuchs E. Ablösung der Aderhaut nach Staaroperation. Graefe's Archive for Clinical and Experimental Ophthalmology 1900;51.
32. Gills JP, Paterson CA, Paterson ME. Mode of action of cyclodialysis implants in man. Invest Ophthalmol 1967;6:141-4.
33. Seetner A, Morin JD. Healing of trabeculectomies in rabbits. Can J Ophthalmol 1979;14:121-5.

34. Toris C. Chapter 7 Aqueous Humor Dynamics I: Measurement Methods and Animal Studies. Current Topics in Membranes2008:193-229.
35. Loewen N, Bahler C, Teo WL, et al. Preservation of aqueous outflow facility after second-generation FIV vector-mediated expression of marker genes in anterior segments of human eyes. Invest Ophthalmol Vis Sci 2002;43:3686-90.
36. Lee MR, Kwon KW, Jung H, et al. Direct differentiation of human embryonic stem cells into selective neurons on nanoscale ridge/groove pattern arrays. Biomaterials 2010;31:4360-6.
37. Xie C, Hu J, Ma H, et al. Three-dimensional growth of iPS cell-derived smooth muscle cells on nanofibrous scaffolds. Biomaterials 2011;32:4369-75.
38. Russell P, Gasiorowski JZ, Nealy PF, Murphy CJ. Response of human trabecular meshwork cells to topographic cues on the nanoscale level. Invest Ophthalmol Vis Sci 2008;49:629-35.
39. Kim DH, Lipke EA, Kim P, et al. Nanoscale cues regulate the structure and function of macroscopic cardiac tissue constructs. Proc Natl Acad Sci U S A 2010;107:565-70.
40. McGahan MC, Bito LZ, Myers BM. The pathophysiology of the ocular microenvironment. II. Copper-induced ocular inflammation and hypotony. Exp Eye Res 1986;42:595-605.
41. Soratur S. Essentials of Dental Materials. New Delhi, India: Jaypee Brothers Medical Publishers; 2002.
42. Dasari A, Rohrmann J, Misra RDK. Micro- and Nanoscale Evaluation of Scratch Damage in Poly(propylene)s. Macromolecular Materials and Engineering 2002;287:889-903.
43. Malihi M, Sit AJ. Effect of head and body position on intraocular pressure. Ophthalmology 2012;119:987-91.
44. Grippo TM, Liu JH, Zebardast N, Arnold TB, Moore GH, Weinreb RN. Twenty-four-hour pattern of intraocular pressure in untreated patients with ocular hypertension. Invest Ophthalmol Vis Sci 2013;54:512-7.
45. Mansouri K, Weinreb RN, Liu JH. Effects of aging on 24-hour intraocular pressure measurements in sitting and supine body positions. Invest Ophthalmol Vis Sci 2012;53:112-6.
46. Lim KS, Wickremasinghe SS, Cordeiro MF, Bunce C, Khaw PT. Accuracy of intraocular pressure measurements in new zealand white rabbits. Invest Ophthalmol Vis Sci 2005;46:2419-23.
47. Mermoud A, Baerveldt G, Minckler DS, Lee MB, Rao NA. Measurement of rabbit intraocular pressure with the Tono-Pen. Ophthalmologica 1995;209:275-7.
48. Eisenberg DL, Sherman BG, McKeown CA, Schuman JS. Tonometry in adults and children. A manometric evaluation of pneumatonometry, applanation, and TonoPen in vitro and in vivo. Ophthalmology 1998;105:1173-81.
49. Acosta AC, Espana EM, Nose I, et al. Estimation of intraocular pressure in rabbits

with commonly used tonometers. Ophthalmic Surg Lasers Imaging 2007;38:43-9.
50. Brandt JD, Gordon MO, Gao F, et al. Adjusting intraocular pressure for central corneal thickness does not improve prediction models for primary open-angle glaucoma. Ophthalmology 2012;119:437-42.
51. DeCroos FC, Ahmad S, Kondo Y, et al. Expanded polytetrafluoroethylene membrane alters tissue response to implanted Ahmed glaucoma valve. Curr Eye Res 2009;34:562-7.
52. Al-Mobarak F, Khan AO. Two-year survival of Ahmed valve implantation in the first 2 years of life with and without intraoperative mitomycin-C. Ophthalmology 2009;116:1862-5.
53. Maumenee AE. External filtering operations for glaucoma: the mechanism of function and failure. Trans Am Ophthalmol Soc 1960;58:319-28.
54. Jones R, Rhee DJ. Corticosteroid-induced ocular hypertension and glaucoma: a brief review and update of the literature. Curr Opin Ophthalmol 2006;17:163-7.
55. Hardten DR, Samuelson TW. Ocular toxicity of mitomycin-C. Int Ophthalmol Clin 1999;39:79-90.
56. Prata JA, Minckler DS, Mermoud A, Baerveldt G. Effects of intraoperative mitomycin-C on the function of Baerveldt glaucoma drainage implants in rabbits. J Glaucoma 1996;5:29-38.
57. Takeuchi K, Nakazawa M, Yamazaki H, et al. Solid hyaluronic acid film and the prevention of postoperative fibrous scar formation in experimental animal eyes. Arch Ophthalmol 2009;127:460-4.
58. Leen MM, Witkop GS, George DP. Anatomic considerations in the implantation of the Ahmed glaucoma valve. Arch Ophthalmol 1996;114:223-4.
59. Molteno AC, Fucik M, Dempster AG, Bevin TH. Otago Glaucoma Surgery Outcome Study: factors controlling capsule fibrosis around Molteno implants with histopathological correlation. Ophthalmology 2003;110:2198-206.
60. Georgoulas S, Dahlmann-Noor A, Brocchini S, Khaw PT. Modulation of wound healing during and after glaucoma surgery. Prog Brain Res 2008;173:237-54.
61. Loeffler KU, Jay JL. Tissue response to aqueous drainage in a functioning Molteno implant. Br J Ophthalmol 1988;72:29-35.
62. Radius RL, Herschler J, Claflin A, Fiorentino G. Aqueous humor changes after experimental filtering surgery. Am J Ophthalmol 1980;89:250-4.
63. New World Medical I. The Ahmed Glaucoma Valve: Introducing the all new Model M4. http://www.ahmedvalve.com/PDF/Flyers/M4_flyer.pdf; 2012.